

Lagrangian Tetrad Dynamics and the Phenomenology of Turbulence.

Michael Chertkov^{1,3}, Alain Pumir² and Boris I. Shraiman³

¹ *Department of Physics, Princeton University, Princeton, NJ 08544*

² *I. N. L. N., 1361 route des Lucioles, F-06560, Valbonne, France*

³ *Bell Labs, Lucent Technologies, 700 Mountain Ave, Murray Hill, NJ 07974*

A new phenomenological model of turbulent fluctuations is constructed by considering the Lagrangian dynamics of 4 points (the *tetrad*). The closure of the equations of motion is achieved by postulating an *anisotropic*, i.e. tetrad shape dependent, relation of the local pressure and the velocity gradient defined on the tetrad. The non-local contribution to the pressure and the incoherent small scale fluctuations are modeled as Gaussian white "noise". The resulting stochastic model for the coarse-grained velocity gradient is analyzed approximately, yielding predictions for the probability distribution functions of different 2nd and 3d order invariants. The results are compared with the direct numerical simulation of the Navier-Stokes. The model provides a reasonable representation of the non-linear dynamics involved in energy transfer and vortex stretching and allows to study interesting aspects of the statistical geometry of turbulence, e.g. vorticity/strain alignment. In a state with a constant energy flux (and K41 power spectrum) it exhibits the anomalous scaling of high moments associated with formation of high gradient sheets - events associated with large energy transfer. An approach to the more complete analysis of the stochastic model, properly including the effect of fluctuations, is outlined and will enable further quantitative juxtaposition of the model with the results of the DNS.

I. INTRODUCTION

The old problem of hydrodynamic turbulence has in recent years attracted resurgent interest stimulated by the new generation of laboratory experiments and the newly acquired ability of the direct numerical simulations to probe interesting aspects of turbulence. In the light of the new ideas and developments there has also been new appreciation of the seminal contributions of Kolmogorov, reviewed in a recent book by Frisch [1], and of Kraichnan to whom the present volume and this article are dedicated. The key issues and the progress of the last years have been well reviewed [1,2] and are well represented in the present Festschrift. Much effort has been dedicated to 1) documenting and understanding the anomalous (i.e. non-Kolmogorov 41) scaling of high moments [1-6] associated with intermittency, 2) understanding the structure and the local geometry of the intermittent regions of the flow [7-15]. On the theory side new ideas derived from the new understanding of anomalous scaling of the Passive Scalar problem [16-20] and of the Burger's turbulence [6,21-23] both pioneered by Kraichnan [24]. Yet, the theoretical description of turbulence based on first principles, i.e. on a controlled approximation to the Navier-Stokes equations, is still over the horizon and to proceed in the right direction one must rely on phenomenology. One reason for pursuing the modeling approach is the need to bridge the existing gulf between our understanding of the scaling [1,2] of turbulent fluctuations and their structure or "statistical geometry" [15,25]. A step in this direction will be the subject of the present paper.

Our goal here is to advance a phenomenological model for the probability distribution function (PDF) of turbulent velocity fluctuations. We shall start by noting that the longitudinal velocity difference between two observation points [26], while being most readily observable, seems a poor candidate for a fundamental dynamical field in terms of which to attempt a closed statistical description. The intuitive reason is that the longitudinal velocity difference senses only one of the 8 locally independent components of the velocity gradient tensor which govern the dynamics of the velocity field. Instead we shall choose the fundamental field to be the coarse grained velocity gradient tensor $M_{ab} \equiv \int_{\mathbf{\Gamma}} d\vec{r} \partial_a v_b(\vec{r})$ defined over a region $\mathbf{\Gamma}$ with characteristic scale R lying in the inertial range. This region may be best thought of as a local correlation volume of the velocity gradient coarse-grained on scale R - an "eddy" of sort. The phenomenological model then will be based on the Lagrangian dynamics of the $\mathbf{\Gamma}$ -volume, parametrized by four points - the "tetrad" - and its strain and vorticity fields as described by M_{ab} . Effort will be made to preserve the

essential non-linear dynamics governing evolution of coarse grained strain and vorticity and the concomitant distortion of the Lagrangian volume. This dynamics expresses the fundamental constraints due to the conservation of energy and circulation. In contrast, the dynamics of velocity fluctuations arising from the scales smaller than that of the tetrad (and generating incoherent motion of the points) will be modeled as a Gaussian white process obeying K41 scaling. Essential element of the theory advanced below will be the decomposition of the pressure into the local part determined by the M-field via incompressibility and the non-local part due to the contribution of distant regions, which will again be modeled as a Gaussian random force. Such an approximation for the pressure may perhaps be justifiable in large spatial dimension [27–29,19], but we shall be content with exploring its consequences and comparing the results with the direct numerical simulations.

We cannot hope to review here the evolution of the phenomenological modeling ideas, yet we shall put the present work into the context of two recent efforts. The "PDF models" of Pope and coworkers [30] attempt to close the equation for the velocity probability distribution function (PDF) on the level of *one* point: in contrast, our model deals with relative velocity differences on 4 points which naturally brings in Kolmogorov's ideas and allows to address the intermittency phenomenon. The two approaches however share the need to model the pressure Hessian/strain-rate correlations (in our case on the coarse-grained level) and share the realization that this model is improved by incorporating dynamical information about local anisotropy [31,32] (in our case furnished by the moment of inertia tensor of the evolving Lagrangian volume). Another point of reference is the *two – point* PDF closure advanced by Yakhot [29] on the basis of the work of Kraichnan [16] and Polyakov [21]. There too one arrived at a Fokker-Planck type equation for the PDF of velocity differences at given point separation, yet the approach differs from the present one in the treatment of the correlations of large and small scale fluctuations and our approach, by virtue of tracking a tetrad rather than a pair will retain more of the geometry of the flow.

The model will be presented in Section 2 in the form of the stochastic equations of motion for two tensors specifying the coarse-grained velocity gradient and the shape (i.e. moment of inertia) of the evolving Lagrangian volume. We shall write down the corresponding Fokker-Planck equation for the Probability Distribution Function and discuss the energy transfer considerations which played the key role in the formulation of the model. Section 3 relates the deterministic aspects of the model to the so called Restricted Euler (RE) dynamics that has been investigated by Vieillefosse [33] originally in the context of the finite time singularities (see also Léorat [34]) and Cantwell and coworkers [35–37] with the emphasis on the local topology of the flow. RE describes the evolution of the velocity gradient at a point within an isotropic approximation for the pressure which allows to close the Euler equation locally. We shall see that elevation of the dynamics to the coarse-grained level and the introduction of the second dynamical field to keep track of the shape of the Lagrangian correlation volume (which depends on the *history* of the strain) allows to go beyond the isotropic pressure approximation: the unphysical finite time singularity of RE is removed, while the sensible short time dynamical properties (related for example to the vorticity strain alignment [8]) are retained. Finally in Section 3 the deterministic dynamics will be compared with the empirical "mean field" equation of motion for the coarse grained velocity tensor \mathbf{M} , constructed from the conditional average $\langle \dot{\mathbf{M}} | \mathbf{M} \rangle$ measured in the DNS of the Navier-Stokes at $R_\lambda = 85$. In Section 4 we return to the stochastic model and write down the formal solution of the Fokker-Planck equation in terms of the path integral relating the probability of a given coarse grained velocity gradient on a given inertial range tetrad to the velocity PDF on the integral scale. This path integral representation serves as a point of departure for the semiclassical approximation. It also has a well defined deterministic limit where the effect of the stochastic terms in the tetrad dynamics can be neglected. In the latter limit the probability of "observing" any given coarse-grained velocity gradient on an inertial range tetrad is determined by the probability of its integral scale preimage and can be calculated by integrating the equations of motion backward in time. This crude but simple approximation is employed in Section 5 in order to gain insight into the behavior of the model and to elaborate its statistical predictions emphasizing energy transfer, enstrophy and its production and the alignment of vorticity and strain. The comparison of the results with the direct numerical simulation of the Navier-Stokes equations is quite encouraging. The calculated probability distribution function also exhibits anomalous scaling of high moments. In conclusion, Section 6 is a summary and the outline of further inquiry.

II. THE MINIMAL MODEL

The minimal parametrization of the Γ volume is a tetrahedron (more generally a d -dimensional simplex) defined by four, hence *tetrad*, (or $d + 1$) Lagrangian points, $\vec{r}_\alpha(t)$, which upon elimination of the center of mass define a triad of vectors $\vec{\rho}_i$: $\vec{\rho}_1 = (\vec{r}_1 - \vec{r}_2)/\sqrt{2}$, $\vec{\rho}_2 = (\vec{r}_1 + \vec{r}_2 - 2\vec{r}_3)/\sqrt{6}$, $\vec{\rho}_3 = (\vec{r}_1 + \vec{r}_2 + \vec{r}_3 - 3\vec{r}_4)/\sqrt{12}$. It will be useful to treat this triad of vectors as 3×3 matrix, ρ_i^a , where a is the spatial index. Analogously, by eliminating the center of mass velocity from the instantaneous velocity of the vertices, \dot{r}_α , one can define a triad of relative velocities, \vec{v}_i . The coarse grained gradient field can now be defined simply by interpolation:

$$M_{ab} = (\rho^{-1})_i^a v_i^b - \frac{\delta_{ab}}{3} \text{tr}(\rho^{-1}v). \quad (1)$$

Alternatively and more generally one may decompose the "observed" velocity differences, v_i^a into a slow component arising from the scales greater than the radius of gyration, $\geq R$, represented by the coarse grained velocity gradient matrix M_{ab} and the rapidly fluctuating incoherent component, u_j^a arising from scales $\ll R$.

$$v_i^a = \rho_i^b M_{ab} + u_i^a. \quad (2)$$

The strategy will be to derive the dynamics of M_{ab} and ρ_i^a while treating \mathbf{u} as a Gaussian white noise with the statistics depending on the Kolmogorov's energy dissipation rate ϵ as well as the instantaneous ρ and \mathbf{M} . Lagrangian dynamics is governed by $\frac{D}{Dt}\mathbf{v}_i = -\nabla p_i + \mathbf{f}_i$ and $\frac{D}{Dt}\rho_i = \mathbf{v}_i$, where \mathbf{f}_i is the random external force and ∇p_i is the pressure gradient, both properly differenced between the observation points. The dynamics of the coarse grained velocity gradient tensor, \mathbf{M} , and the tetrad tensor ρ has the form:

$$\frac{d}{dt}M_{ab} + M_{ab}^2 - \Pi_{ab} \text{tr}M^2 = \xi_{ab}, \quad (3a)$$

$$\frac{d}{dt}\rho_i^a - \rho_i^b M_{ba} = u_i^a, \quad (3b)$$

$$\Pi_{ab} \equiv k_i^a k_i^b / \text{tr} \mathbf{k} \mathbf{k}^\dagger, \quad (3c)$$

with matrix $\mathbf{k} \equiv \rho^{-1}$. The left hand sides of (3a,3b) describe the self-advection and stretching of the tetrad by the coherent (on the scale of ρ) component of the velocity field. The right hand side of (3a) derives from the pressure gradient and the random force differences as well as from the coupling to incoherent small scale fluctuations. The $\Pi_{ab} \text{tr}M^2$ term, with $\text{tr}\Pi = 1$ on the left hand side represents the "local" component of the pressure needed to insure conservation of $\text{tr}\mathbf{M} = 0$ as required by incompressibility. Tensor Π_{ab} is a measure of tetrad anisotropy representing the anisotropy of the Lagrangian correlation volume built up by prior evolution [38]. This choice of the local term, in contrast with the simpler, isotropic form [33] is dictated by the requirement that the pressure forces should do no work and drop out of the energy balance (see below). In addition it reintroduces proper reduction of the deterministic dynamics (left hand side of (3a)) to 2D: i.e. a 2D velocity gradient configuration remains 2D provided that the tetrad has the shape of a filament, i.e. $\rho^\dagger \rho$ is a tensor of rank one. The remaining non-local part of the pressure is subsumed in ξ_{ab} .

We now define the stochastic components of the model appearing on the right hand sides of (3a-b). It is appealing to model the non-local part of the pressure retained in ξ , along with the contribution of small scales, as δ -correlated Gaussian random noise with the variance depending on the energy flux ϵ as well as the instantaneous ρ and \mathbf{M} . Let us consider a polynomial :

$$\xi = \eta + \zeta \mathbf{M} + \alpha(\mathbf{M}^2 - \Pi \text{tr} \mathbf{M}^2). \quad (4)$$

where η is a random matrix, and ζ a random function. The dimension of both ξ and \mathbf{M}^2 is time^{-2} so that α is a constant. The last term is clearly not the most general one can write. It is however the one suggested by the numerical study of the statistics of the right hand side of (3a), originally by Borue and Orszag [39]. According to the DNS the average ξ_{ab} conditioned on \mathbf{M} is not zero, but is reasonably well approximated by $\alpha(\mathbf{M}^2 - \Pi \text{tr} \mathbf{M}^2)$ with $0 < \alpha < .8$, depending on the scale, at least for the isotropic tetrad (i.e. $\Pi = 1/3$). We shall assume that in the inertial range α is constant (which corresponds to keeping only the deterministic component of the 3d term in (4)) and take it to be a model parameter. This α term "renormalizes" the time scale of the deterministic dynamics described by the left hand side of the equation (3a) and will have an important consequence for the energy transfer in the model, as we shall see shortly.

Let

$$\langle \eta_{ab}(t) \eta_{cd}(0) \rangle = \frac{2C_\eta \epsilon}{\text{tr} \rho \rho^\dagger} [\delta_{ac} \delta_{bd} - \frac{1}{3} \delta_{ab} \delta_{cd}] \delta(t) \quad (5a)$$

which is the simplest form respecting incompressibility, with Kolmogorov's energy flux ϵ and C_η - a dimensionless parameter. Random η causes diffusion in velocity space; note that ϵ has the dimension of corresponding diffusivity. The appearance of ϵ in (5a) is further supported by the fact that η fluctuations contribute to the energy transfer as we shall see below. In the "minimal" model, which we are now constructing we shall drop the possible multiplicative random field ζ (see Eq.(4)).

The fluctuations of the small scale [40] \mathbf{u} can be resolved into parts which are longitudinal and transverse to ρ_i^a :

$$\langle u_i^a(t) u_j^b(0) \rangle = 2C_{||} \sqrt{tr \mathbf{M} \mathbf{M}^\dagger} \rho_i^a \rho_j^b \delta(t) + 2C_{\perp} \sqrt{tr \mathbf{M} \mathbf{M}^\dagger} (\rho^2 \delta^{ab} \delta_{ij} - \rho_i^a \rho_j^b) \delta(t) \quad (5b)$$

where with the K41 scaling in mind we take the characteristic time to be the "eddy turnover" time, $1/\sqrt{tr \mathbf{M} \mathbf{M}^\dagger}$. The longitudinal part of \mathbf{u} in the ρ -equation (3b) would by itself produce Richardson diffusion behavior, $\langle \rho^2(t) \rangle \sim \epsilon t^3$ provided that the Kolmogorov scaling $\sqrt{tr \mathbf{M} \mathbf{M}^\dagger} \sim \epsilon^{1/3} \rho^{-2/3}$ holds. However, Richardson diffusion would also arise from the non-Gaussian coherent stretching term $\rho \mathbf{M}$, and the Gaussian longitudinal fluctuations, $C_{||}$, do not appear to be essential. We shall set $C_{||} = 0$. The transverse fluctuations C_{\perp} however are very important, because in their absence the effect of volume preserving coherent stretching would lead to the rapid growth of anisotropy of the tetrad. The incoherent transverse velocity fluctuations act to redistribute the vertices of the tetrad uniformly on the surface of the $\rho^2 \equiv tr \rho^\dagger \rho$ hyper-sphere in $d^2 = 9$ dimensions, thus introducing the isotropisation mechanism. The competition of the coherent stretching which leads to the growth of the radius of gyration ρ^2 (both forward and backward in time) and the isotropisation over the ρ^2 shell will play the key role in setting up the energy flux.

The stochastic tetrad dynamics defined by Eq. (3-5) determines the Lagrangian transition probability from tetrad (\mathbf{M}', ρ') to (\mathbf{M}, ρ) at a time t later, $G_t(\mathbf{M}, \rho | \mathbf{M}', \rho')$, which satisfies a Fokker-Planck equation

$$\left(\frac{\partial}{\partial t} - \mathbf{L} \right) G_t(\mathbf{M}, \rho | \mathbf{M}', \rho') = \delta(\mathbf{M} - \mathbf{M}') \delta(\rho - \rho') \quad (6)$$

with the evolution operator

$$\begin{aligned} \mathbf{L} = & (1 - \alpha) \frac{\partial}{\partial M_{ab}} (M_{ab}^2 - \Pi_{ab} tr \mathbf{M}^2) - \frac{\partial}{\partial \rho_b^i} \rho_a^i M_{ab} \\ & + C_\eta \frac{\epsilon}{\rho^2} \left(\frac{\partial^2}{\partial M_{ab} \partial M_{ab}} - \frac{1}{3} \frac{\partial^2}{\partial M_{aa} \partial M_{bb}} \right) + C_{\perp} \sqrt{tr \mathbf{M} \mathbf{M}^\dagger} \frac{\partial}{\partial \rho_i^a} (\rho^2 \delta^{ab} \delta_{ij} - \rho_i^a \rho_j^b) \frac{\partial}{\partial \rho_j^b}. \end{aligned} \quad (7)$$

The invariant joint distribution, $P(\mathbf{M}, \rho)$, satisfying

$$\partial_t P(\mathbf{M}, \rho) = \mathbf{L} P(\mathbf{M}, \rho) = 0 \quad (8)$$

can be interpreted as the Eulerian PDF $P(\mathbf{M}, \rho)$ provided that the normalization $\int d\mathbf{M} P(\mathbf{M}, \rho) = 1$ is imposed [42]. Equations (7-8) once supplemented with the boundary condition specifying the Eulerian PDF on the integral scale, $\rho^2 = L^2$, completely define our model.

Before proceeding with the analysis of the Fokker-Planck equation (8), let us examine the energy balance, which was one of the key consideration in the formulation of the model:

$$\begin{aligned} \frac{1}{2} \partial_t \langle tr \mathbf{V} \mathbf{V}^\dagger \rangle_\rho & \equiv \int d\mathbf{M} tr(\rho \mathbf{M} \mathbf{M}^\dagger \rho^\dagger) \partial_t P(\mathbf{M}, \rho) \\ & = - \frac{\partial}{\partial \rho_a^i} \langle V_a^i tr(\mathbf{V} \mathbf{V}^\dagger) \rangle_\rho + \alpha \langle tr(\mathbf{V} \mathbf{V}^\dagger \mathbf{M}) \rangle_\rho \\ & \quad + \frac{16}{3} C_\eta \epsilon - C_{\perp} D_d + C_{\perp} f, \end{aligned} \quad (9)$$

which is obtained by multiplying eq (8) by $tr \mathbf{V} \mathbf{V}^\dagger$ (where $V_a^i \equiv \rho_b^i M_{ba}$) and averaging with respect to \mathbf{M} . Note that the average $\langle \dots \rangle_\rho$ is taken at fixed ρ and remains a function of it. The first two terms on the right hand side may be identified as the divergence of the large scale energy flux and the eddy damping respectively.

Note that the term originating from the deterministic component of the pressure $\Pi_{ab} tr \mathbf{M}^2$ drops out: the particular form of Π_{ab} was chosen for that purpose on the grounds that the pressure gradients should not contribute to the energy transfer as seen in the von Kármán-Howarth derivation [43]. However, since V_a^i is only the coarse grained and not the full local velocity, in contrast with the von Kármán - Howarth analysis the divergence of the energy flux is balanced not directly by the viscous dissipation term, but by the eddy damping. There are also additional contributions due to the coupling with small scale fluctuations represented by the last three terms in (9). The C_η term represents the *diffusive* component of the energy flux arising from the small scale fluctuations and the coupling of the tetrad to the neighboring regions (entering via Gaussian η). The $C_{\perp} f$ term represents the transverse energy flux with:

$$f = \frac{\partial}{\partial \rho_i^a} (\rho^2 \delta^{ab} \delta_{ij} - \rho_i^a \rho_j^b) \left[\frac{\partial}{\partial \rho_j^b} \left\langle \sqrt{tr \mathbf{M} \mathbf{M}^\dagger} tr \mathbf{V} \mathbf{V}^\dagger \right\rangle_\rho - 2\rho_j^c \left\langle \sqrt{tr \mathbf{M} \mathbf{M}^\dagger} (\mathbf{M} \mathbf{M}^\dagger)_{bc} \right\rangle_\rho \right] \quad (10)$$

which redistributes the energy within the $\rho^2 = \text{const}$ shell, while the $C_\perp D_d$ is the diffusive contribution to the eddy damping:

$$D_d = 18 \left\langle \sqrt{\text{tr} \mathbf{M} \mathbf{M}^\dagger} \text{tr} \left[\left(\rho^\dagger \rho - \frac{1}{3} \rho^2 \right) \mathbf{M} \mathbf{M}^\dagger \right] \right\rangle_\rho. \quad (11a)$$

This D_d is reminiscent of the Smagorinsky [44,39] form of eddy damping (popular in sub-grid simulations [44,45]) but with significant difference that in the latter the d -wave projector $(\rho^\dagger \rho - \frac{1}{3} \rho^2)$ appearing in (11a) is replaced by the simple scale factor ρ^2 . Hence, in contrast with the Smagorinsky model, our diffusive damping term is only active to the extent that the $\left\langle \sqrt{\text{tr} \mathbf{M} \mathbf{M}^\dagger} (\mathbf{M} \mathbf{M}^\dagger)_{ab} \right\rangle_\rho$ tensor is correlated with $(\rho^\dagger \rho)_{ab}$ tensor within the ρ^2 shell. Strictly speaking D_d is not positive definite and its interpretation as the *damping* term is contingent on the expectation that the tetrad dynamics builds up the alignment of the principal axis of $\rho^\dagger \rho$ and $\mathbf{M} \mathbf{M}^\dagger$.

Notably, the deterministic eddy damping term which has appeared in (9)

$$D_{nl} = -\alpha < \text{tr} \mathbf{V}^\dagger \mathbf{V} \mathbf{M} >_\rho \quad (11b)$$

is a direct generalization of the so-called *non-linear* eddy damping $\rho^2 < \text{tr} \mathbf{M}^2 \mathbf{M}^\dagger >$ advanced by Bardina et al. [46] and reduces to it for isotropic tetrads $\rho \rho^\dagger = \mathbf{1} \rho^2$. In this limit $D_{nl} \rightarrow -\text{tr}(\mathbf{s}^3 - \boldsymbol{\Omega} \cdot \mathbf{s} \cdot \boldsymbol{\Omega})$, where \mathbf{s} and $\boldsymbol{\Omega}$ are respectively the symmetric and antisymmetric parts of \mathbf{M} . Thus the energy transfer down scale is due to negative strain skewness or positive enstrophy production [26,1] (i.e. vortex stretching). We can define the energy flux by averaging over the fixed ρ^2 shells. Let $R \equiv \sqrt{\rho^2}$ and $V_R \equiv \rho_i^a V_i^a / R$ denote the longitudinal velocity, then

$$\epsilon = -\partial_R \left\langle \mathbf{V}_R \text{tr} \mathbf{V} \mathbf{V}^\dagger \right\rangle_R + \frac{16}{3} C_\eta \epsilon \quad (12)$$

is balanced by eddy damping $\epsilon = D_{nl} + C_\perp D_d$. Here $\langle \dots \rangle_R$ denotes an additional average over $\rho^2 = R^2$ shell.

Below we will often think of the diffusive contributions as being small compared to the non-linear interactions on current scale: that is, we shall assume $C_\eta, C_\perp \ll 1$ and treat them as (a singular) perturbation of the deterministic dynamics. Another tractable and perhaps physically more plausible limit is $C_\perp \gg 1$.

III. DETERMINISTIC DYNAMICS AND THE RESTRICTED EULER MODEL.

Note that the equation of the form (3a) also governs the Lagrangian evolution of the actual *local* velocity gradient matrix $m_{ab} = \partial_a v_b$ (we use lower case \mathbf{m} to avoid confusion with the coarse grained object)

$$\frac{d}{dt} m_{ab} + m_{ab}^2 = -\partial_a \partial_b p \quad (13a)$$

as derives from the Euler equation. Léorat [34] and Vieillefosse [33] have considered (13a) retaining only the *local* and *isotropic* contribution to the pressure

$$\partial_a \partial_b p = -\frac{\delta_{ab}}{3} \text{tr} \mathbf{m}^2 \quad (13b)$$

as a model of vorticity dynamics and observed that (13a,13b) leads to a finite time singularity with $\|\mathbf{m}\| \sim (t_* - t)^{-1}$. The dynamics governed by (13a,13b) - the "Restricted Euler dynamics", to use Cantwell's terminology [35] lies entirely in the two-dimensional phase space defined by the two invariants [33,35] $\text{tr} \mathbf{m}^2$ and $\text{tr} \mathbf{m}^3$. This reduction stems from the $SL(3)$ invariance, $\mathbf{m} \rightarrow \mathbf{g} \mathbf{m} \mathbf{g}^{-1}$ with \mathbf{g} being an arbitrary 3×3 matrix, which allows one to bring $\mathbf{m}(t)$ to diagonal form $\boldsymbol{\Lambda}(t)$ by a *time independent* similarity transformation $\mathbf{m}(t) = \mathbf{U} \boldsymbol{\Lambda}(t) \mathbf{U}^{-1}$. There is yet one more independent constant of motion found by Vieillefosse [33]: the "discriminant" $D \equiv 3(\text{tr}(\mathbf{m}^3))^2 - \frac{1}{2}(\text{tr}(\mathbf{m}^2))^3 = -(\lambda_1 - \lambda_2)^2(\lambda_2 - \lambda_3)^2(\lambda_3 - \lambda_1)^2$, where $\lambda_i(t)$ are the (in general complex) eigenvalues of $\mathbf{m}(t)$. The RE dynamics thus reduces to 1D flow, i.e. it is integrable! Figure 2 shows the flow in the 2D phase plane of the Cantwell's invariants [35] $Q \equiv -\frac{1}{2} \text{tr} \mathbf{m}^2$, $R \equiv -\frac{1}{3} \text{tr} \mathbf{m}^3$ and the finite time singularity corresponds to the $R \rightarrow \infty$, $Q \rightarrow -\infty$ asymptotically approaching the $D = 0$ separatrix.

Along the $D = 0$ separatrix the flow is particularly simple:

$$\mathbf{m}(t) = \begin{pmatrix} \lambda(t) & 0 & 0 \\ 0 & \lambda(t) & 0 \\ 0 & 0 & -2\lambda(t) \end{pmatrix} \quad (14)$$

with $\lambda(t) = \lambda(0)/(1 - t\lambda(0))$ making the finite time singularity at $t_* = 1/\lambda(0)$ explicit.

The region above the separatrix, $D > 0$, is elliptic: the eigenvalues of the velocity gradient eigenvalues become complex and the Lagrangian trajectories are rotating; the region below the separatrix, $D < 0$, is hyperbolic: the eigenvalues are real and the trajectories are strain dominated. These topological aspects of RE dynamics were emphasized by Blackburn et al [37].

As a model of finite time singularity RE solutions were rejected [47] on the reasonable ground that if considered as global solutions of Euler equations these do not satisfy sensible boundary conditions and have unbounded energy. Ashurst et al [8] however noted that the statistics of the vorticity/strain alignment observed in the DNS of Navier-Stokes may be qualitatively understood in terms of RE. Subsequently Cantwell and coworkers [35–37] proceeded to investigate the DNS generated statistics of R, Q invariants and observed that the probability distribution function (PDF) of R, Q exhibits a pronounced tail along the Vieillefosse $D = 0$ asymptote as can be seen on Fig.3. These two observations suggest that despite the draconian local and isotropic approximation to pressure and the unphysical finite time singularity the RE dynamics does capture certain statistical features of the physical flow.

The deterministic part of the Lagrangian tetrad dynamics defined in Section 2 generalizes RE by reinterpreting the velocity gradient tensor as a coarse-grained field defined over the tetrad ρ and completing the Lagrangian picture by adding the dynamical equation for $\rho(t)$. The ρ field introduces the measure of current length scale and the dependence on the history of the strain which controls the "shape" of the tetrad. The ρ -dynamics (3b) is coupled to \mathbf{M} via the anisotropy tensor $\mathbf{\Pi}$. For an isotropic tetrad (i.e. regular tetrahedron) $\Pi_{ab} = \delta_{ab}/3$ and the M -dynamics (the left hand side of (3a)) reduces instantaneously to RE equation (13a,13b). In the next instant however the tetrad will become distorted through the action of the volume preserving \mathbf{M} following the ρ -dynamics equation (left hand side of (3b)) and the trajectory will come out of the RE plane. Its evolution will depart from RE as the anisotropy increases and at some point the growth of $||\mathbf{M}||$ will be cut off. This is most easily seen for the $D = 0$ Vieillefosse line. The dynamics of λ (see (14)) becomes $\dot{\lambda} = (6q^{-1} - 1)\lambda^2$, with $\mathbf{\Pi} = \text{diag}\{1, 1, q - 2\}/q$ where q evolves according to $\dot{q} = 6(q - 2)\lambda$. The isotropic tetrad corresponds to $q = 3$. Starting from isotropy and $\lambda > 0$ both $\lambda(t)$ and $q(t)$ grow. The growth of q corresponds to the contraction of one of the principle axis of the $\rho^\dagger \rho$ tensor as the tetrad is flattened in a pancake. However when $q > 6$ the growth of λ reverses. Thus, anisotropy caused by the stretching of the tetrad cuts off the Vieillefosse finite time singularity [48]. The modified RE dynamics however retains the initial growth of \mathbf{M} with two expanding and one contracting strain directions and the consequent deformation of the tetrad into a pancake or ribbon. [49] This process is the fundamental step of energy transfer [26,50]. In the next Section we will see that the Vieillefosse tail (large $R > 0, Q < 0$ region) of the Cantwell PDF on Fig.3 which is generated through this process, indeed corresponds to large negative strain skewness associated with the energy transfer [26]. Another retained aspect of the RE dynamics is the evolution of the vorticity/strain alignment from configurations where vorticity is parallel to α -strain (i.e. the fast stretching direction) to configuration where vorticity is aligned with the intermediate, β -strain as observed numerically [7,51,8]. The new feature of the modified model is that while in the isotropic RE all 2D configurations of \mathbf{M} evolve into 3D, (e.g. $M_{ab} = \epsilon_{abz}\omega_z$ will in the next instant acquire, due to low local pressure, a contracting component of strain acting along the z -direction which will act to destroy ω_z), the new anisotropic model allows the 2D configurations of \mathbf{M} to persist provided that the $\mathbf{\Pi}$ tensor is rank two ($\rho^\dagger \rho$ rank one) which correspond to filament like tetrads. Note that both intense vorticity and quasi-one dimensional tetrads will be produced by the action of strain with one stretching and two contracting directions $\text{tr}[\mathbf{s}^3] > 0$, thus there potentially is a chance of describing vortex "worms" [7,9,11,12]. We shall return to the discussion of the kinematics of energy transfer and vortex stretching in Section 5.

How can one compare the deterministic tetrad dynamics model with the real Navier-Stokes dynamics ? The relevant empirical object is the average $d\mathbf{M}/dt$ and $d\rho/dt$ conditioned on \mathbf{M}, ρ but to simplify matters we will restrict to isotropic tetrads and examine the flow in the Q, R phase space generated by the conditional averages $\langle \dot{R}|R, Q \rangle$ and $\langle \dot{Q}|R, Q \rangle$. The latter were obtained by a DNS of Navier-Stokes.

Briefly, the Navier-Stokes equations are integrated by a standard pseudo-spectral algorithm. Our code is fully de-aliased. We used up to $(128)^3$ collocation grid points, and the effective resolution was maintained to be higher than $k_{\max}\eta \geq 1.4$, where k_{\max} is the highest wave-vector in the simulation, and η_K the Kolmogorov length scale ($\eta_K \equiv (\nu^3/\epsilon)^{1/4}$). Statistics were accumulated for at least 3 eddy turnover times. In the following, we present our results for a Taylor scale $Re_\lambda = 85$. Our investigation of the influence of the Reynolds number in the range $20 \leq Re_\lambda \leq 85$ did not reveal any major qualitative change of the statistics presented here.

Fig. 4a,b,c show the streamlines in the (R, Q) plane, reconstructed from the conditional averages of $\langle \dot{R}|R, Q \rangle$ and $\langle \dot{Q}|R, Q \rangle$ computed numerically for three different ρ^2 . The latter were increasing from the dissipation range to large scale. For isotropic ρ our \mathbf{M} -dynamics is instantaneously tangent to the RE and therefore the empirical flows can be compared with Fig. 2. Remarkably, while there are significant deviations in the topology of the flow for ρ in the

dissipative range (Fig.4a), the instantaneous flow for large scale ρ is surprisingly close to RE. The deviations at small scales are presumably due to the viscous effects. The conditional flow for $|\rho| \geq 10\eta_k$ can be fitted by the modified RE:

$$\frac{d\mathbf{M}}{dt} = (\alpha - 1)(\mathbf{M}^2 - \Pi \text{Tr} \mathbf{M}^2) \quad (15)$$

with α decreasing with increasing $|\rho|/\eta_K$ from .8 to 0. For the reasons related to the energy transfer, discussed in Section 2, we believe that α should be constant in the inertial range. The continuous scale dependence observed in the fit to DNS however is not unexpected, because the inertial range at the accessible Re is quite limited. On the other hand the approximate validity of (15) as a description of the coarse-grained Lagrangian evolution is quite encouraging. It would be important to extend the comparison of the deterministic dynamics (15) with the numerical simulation for anisotropic tetrads, however in that case the $SL(3)$ invariance of (15) is lost and in addition to the R, Q invariants the time derivative must be conditioned on the vorticity, which makes the computation more demanding statistically. It would also be important to investigate systematically the deviations of the conditional flow from (15): these are expected to arise from the possible additional deterministic terms in (15) (e.g. $\gamma\mathbf{M}$) as well as the stochastic dynamics. Much further work is required in this direction.

IV. LAGRANGIAN PATH INTEGRALS AND THE SEMICLASSICAL APPROXIMATION.

Let us now explore the statistical properties of the coarse-grained M -field on the tetrad ρ . The probability distribution $P(\mathbf{M}, \rho)$ is governed by the Fokker-Planck equation (7,8) but requires specification of an additional boundary condition. Since the PDF of velocity is known to be Gaussian on the integral scale we shall fix [52].

$$P(\mathbf{M}, \rho)|_{\rho^2=L^2} \sim \exp \left[-\frac{\text{tr} \mathbf{M} \mathbf{M}^\dagger}{(\epsilon L^{-2})^{2/3}} \right]. \quad (16)$$

To impose the integral scale boundary condition one may use a generalization of Green's theorem

$$\begin{aligned} P(\mathbf{M}', \rho') &= \int d\mathbf{M} \int d\rho [P(\mathbf{M}, \rho) \mathbf{L}^\dagger \mathbf{g}^\dagger(\mathbf{M}, \rho | \mathbf{M}', \rho') - \mathbf{L} P(\mathbf{M}, \rho) \mathbf{g}^\dagger(\mathbf{M}, \rho | \mathbf{M}', \rho')] \\ &= \int d\mathbf{M} \int_{\rho^2=L^2} \text{tr}(d\rho \mathbf{M}^\dagger \rho^\dagger) P(\mathbf{M}, \rho) \mathbf{g}^\dagger(\mathbf{M}, \rho | \mathbf{M}', \rho') \end{aligned} \quad (17)$$

where \mathbf{L}^\dagger denotes the adjoint operator which governs evolution backward in time (obtained by $\mathbf{M} \rightarrow -\mathbf{M}$) and $\mathbf{g}^\dagger(\mathbf{M}, \rho | \mathbf{M}', \rho') = \mathbf{L}^{\dagger-1}$ its static Green function.

The static Green's function \mathbf{g}^\dagger is computed via the Lagrangian Green's function (6):

$$\mathbf{g}^\dagger(\mathbf{M}, \rho | \mathbf{M}', \rho') = \int_{-\infty}^0 dT G_T(\mathbf{M}, \rho | \mathbf{M}', \rho') \quad (18)$$

which has an intuitively appealing path integral representation:

$$G_{-T}(\mathbf{M}, \rho | \mathbf{M}', \rho') = \int_{\mathbf{M}(-T)=\mathbf{M}'}^{\mathbf{M}(0)=\mathbf{M}} D\mathbf{M} \int_{\rho(-T)=\rho'}^{\rho(0)=\rho} D\rho \exp[-S(\{\mathbf{M}, \rho\})] \quad (19)$$

summing over all possible paths connecting initial \mathbf{M}', ρ' at time $-T$ with the final \mathbf{M}, ρ at time 0 weighted with the action

$$\begin{aligned} S &= \frac{1}{2} \int_{-T}^0 dt \left[\frac{\|\dot{\mathbf{M}} - (\alpha - 1)(\mathbf{M}^2 - \Pi \text{tr} \mathbf{M}^2)\|^2}{C_\eta \epsilon \rho^{-2}} \right. \\ &\quad \left. + \frac{\text{tr}[(\dot{\rho} - \rho \mathbf{M}) (C_\perp^{-1}(1 - \hat{\rho} \hat{\rho}^\dagger) + C_\parallel^{-1} \hat{\rho} \hat{\rho}^\dagger) (\dot{\rho} - \rho \mathbf{M})^\dagger]}{\rho^2 \sqrt{\text{tr} \mathbf{M} \mathbf{M}^\dagger}} \right] \end{aligned} \quad (20)$$

where $\|X\|^2 \equiv \text{tr} \mathbf{X} \mathbf{X}^\dagger$, $\hat{\rho} \equiv \rho/|\rho|$ and $C_\parallel \rightarrow 0$, as assumed before.

This path integral form invites a semi-classical approximation [41,54,53] which estimates the integral via the saddle point $G_T(\mathbf{M}, \rho|\mathbf{M}', \rho') \sim \exp[-S_c(\mathbf{M}, \rho|\mathbf{M}', \rho')]$ given by the minimal action S_c along the "classical" trajectories connecting the prescribed initial and final points (in time T) and obeying the Euler-Lagrange variational equations. Moreover, for each final point (\mathbf{M}, ρ) there exists a unique $S = 0$ trajectory governed by the deterministic part of Lagrangian dynamics (3a,3b) which picks out the Lagrangian preimage $\mathbf{M}' = \tilde{\mathbf{M}}(\mathbf{M}, \rho, -T)$, $\rho' = \tilde{\rho}(\mathbf{M}, \rho, -T)$ as an initial condition. If the small scale generated stochastic component of the dynamics were small $C_\perp, C_\eta \rightarrow 0$ these deterministic Lagrangian trajectories would control the Green's function. Since the probability is constant along the zero action trajectory the PDF of the final \mathbf{M}, ρ is determined by the probability of its Lagrangian preimage $\mathbf{M}' = \tilde{\mathbf{M}}(\mathbf{M}, \rho, -T)$ at the integral scale where the PDF is assumed to be Gaussian. Crude as this *zero action* approximation is, it is the natural zeroth order calculation and will provide some physically interesting insights as we shall see below. The full semi-classical analysis will be deferred to a forthcoming publication.

V. PROBABILITY DISTRIBUTION FUNCTIONS AND STATISTICAL GEOMETRY.

To make contact with the numerical results we shall use the "poor man's" zero action approximation introduced in the previous section and according to which the probability of given \mathbf{M} observed on a tetrad ρ in the inertial range is equal to the probability of its integral scale preimage. The latter is found by integrating the deterministic part of the equations of motion (which generates zero action trajectories) from the observation point *backward in time*:

$$\frac{d}{dt}\mathbf{M} = -(\alpha - 1)(\mathbf{M}^2 - \mathbf{\Pi}tr\mathbf{M}^2) \quad (21a)$$

$$\frac{d}{dt}\mathbf{g} = -\mathbf{g}\mathbf{M} - \mathbf{M}^\dagger\mathbf{g}^\dagger - \beta\sqrt{tr\mathbf{M}\mathbf{M}^\dagger}\left(\mathbf{g} - \frac{1}{3}tr\mathbf{g}\right) \quad (21b)$$

where $\mathbf{g} \equiv \rho^\dagger\rho$. The β term has been added to reintroduce the isotropisation effect due to the transverse small scale fluctuations already in the deterministic approximation. This may be thought of as a Mean Field treatment of the C_\perp term in (7) which is physically more appropriate than the formal $C_\perp, C_\eta \rightarrow 0$ deterministic limit of (20). Dimensionless constants α and β will serve as model parameters. Equations (21a,21b) will be integrated back in time until $tr\mathbf{g} = \rho^2$ reaches the integral scale, yielding for the PDF:

$$P(\mathbf{M}, \mathbf{g}) \sim \exp \left[-\frac{tr \left(\mathbf{M}'_L(\mathbf{M}, \mathbf{g})\mathbf{M}'_L{}^\dagger(\mathbf{M}, \mathbf{g}) \right)}{(\epsilon L^{-2})^{2/3}} \right] \quad (22)$$

with $\mathbf{M}'_L(\mathbf{M}, \mathbf{g})$ (and the time of flight T) fixed implicitly by $tr[\tilde{\mathbf{g}}(\mathbf{M}, \mathbf{g}, -T)] = L^2$. To the extent that the non-trivial PDF in this approximation arises as a non-linear mapping of the initially Gaussian variables, our construction here is reminiscent of Kraichnan's "Mapping Closure" [6,55].

Let us now construct the PDF of the R, Q invariants for the isotropic tetrad of radius r . It is convenient to consider the elliptic $D > 0$ and the hyperbolic $D < 0$ regions separately and use different parameterizations of the \mathbf{M} matrix:

a) for $D > 0$

$$\mathbf{M} = \begin{pmatrix} \lambda & \Delta e^\gamma & \omega_2 \\ -\Delta e^{-\gamma} & \lambda & \omega_1 \\ 0 & 0 & -2\lambda \end{pmatrix} \quad (23a)$$

and b) for $D < 0$

$$\mathbf{M} = \begin{pmatrix} \lambda + \Delta & \omega_3 & \omega_2 \\ 0 & \lambda - \Delta & \omega_1 \\ 0 & 0 & -2\lambda \end{pmatrix} \quad (23b)$$

where ω_a refers to vorticity and in (23a) $\omega_3 \equiv 2\Delta \cosh \gamma$. The invariants are a) $R = 2\lambda(\lambda^2 + \Delta^2)$ and $Q = \Delta^2 - 3\lambda^2$ and b) $R = 2\lambda(\lambda^2 - \Delta^2)$ and $Q = -\Delta^2 - 3\lambda^2$ and the strain tensor is $\mathbf{s} \equiv (\mathbf{M} + \mathbf{M}^\dagger)/2$. It is straightforward to numerically integrate (21a,21b) starting with given \mathbf{M} and $\mathbf{g} = r^2\mathbf{1}$ in time until $\frac{1}{3}Tr\mathbf{g} = L^2$ at which point $P(\mathbf{M}, \mathbf{g})$ is assigned via (22). However, to determine $P_r(R, Q)$ one must integrate $P(\mathbf{M})$ over a) $\gamma, \omega_{1,2}$ and b) over $\tilde{\omega}$. (Note the Jacobian: $\int d\mathbf{M}\delta(tr\mathbf{M}) = \int dRdQd\tilde{\omega} = \int d\lambda d\Delta d\tilde{\omega} \sqrt{|D|}$ and $d\Delta d\omega_1 = 2\Delta\gamma \sinh[\gamma] d\gamma d\Delta$).

The task is simplified within the saddle approximation where the integration is reduced to minimization [56] of $\log P(\mathbf{M}, \mathbf{r})$ with respect to the integration variables which we carry out numerically via an "amoeba" algorithm [57]. Over the whole R, Q plane we find that the saddle point is at a) $\gamma = \omega_{1,2} = 0$ and b) $\vec{\omega} = 0$. In addition for the special case of $D = 0$, when λ is the only non-zero parameter in (23a,23b) the trajectory and the $P(\mathbf{M}, \mathbf{g})$ can be computed analytically (see Appendix A). The resulting distribution (for different r) is displayed on Fig. 5a,b. $P(Q, R)$ exhibits a long (but Gaussian $\sim \exp(-a\lambda^2 r^{2\gamma+})$) ridge - the "Vieillefosse tail" - along the $D = 0$ line in the $R > 0, Q < 0$ quadrant and a valley of low probability approaching the origin from the $R > 0$ side. This structure appears because the backward in time trajectory of the point on the $D = 0$ separatrix converges to the origin and maps to a highly probable, small \mathbf{M}' integral scale preimage, whereas the trajectories originating in the low probability gulf in their time reversed dynamics are swept westward past the origin into the improbably large \mathbf{M}' region. The PDF $P_r(R, Q)$ evolves continuously with decreasing r/L away from the Gaussian (which appears non-trivial in the R, Q variables) shown for comparison on Fig.6. The appearance of the PDF tail along $D = 0, R > 0$ and the trend of r/L dependence are reminiscent of those for the PDF obtained from the Navier-Stokes. Yet, both high probability ridge and the low probability valley found in the present deterministic approximation are strongly exaggerated. There is a good reason to expect that the effect of the fluctuations will be strong in these regions: the narrow ridge should be largely "washed out" as the asymptotic behavior of the tails and low probability regions is clearly dominated by fluctuations. Yet again, the rather complex R, Q dependence of the PDF and the crude qualitative similarity of the model PDF with the results of the DNS merits a detailed discussion of the underlying kinematics and dynamics.

Let us compute the distribution in R, Q plane of the average enstrophy ω^2 and enstrophy production $\vec{\omega} \cdot \mathbf{s} \cdot \vec{\omega} = \frac{1}{2} \text{Tr}(\mathbf{M} + \mathbf{M}^\dagger)(\mathbf{M} - \mathbf{M}^\dagger)^2$ which measures the rate of vortex stretching [26]. The enstrophy density is defined by $e(R, Q) = \int d\vec{\omega} \omega^2 P_r(R, Q, \omega)$ but in order to save computer time will only be evaluated in the saddle approximation by varying the integrand w.r.t. $\vec{\omega}$. For all of the hyperbolic region the saddle of the integral occurs at a non-zero values of $\gamma, \vec{\omega}$ parameters (21a,21b). The result is presented in Fig.7. We see that the average enstrophy peaks at $R = 0$ and small positive Q . This is explained by noting that the conditional average $\langle \vec{\omega}^2 | R, Q \rangle$ grows like Q (at least for $R \approx 0$ and $Q > 0$) because $Q = (\frac{1}{2}\vec{\omega}^2 - \text{Tr} \mathbf{s}^2)/2$, while $P(R, Q)$ falls off. The average enstrophy production $\sigma(R, Q) \equiv \int d\vec{\omega} \vec{\omega} \cdot \mathbf{s} \cdot \vec{\omega} P_r(R, Q, \vec{\omega})$ is also dominated by a non-trivial saddle and has the R, Q dependence shown in Fig.8. We observe that enstrophy is produced predominantly in the upper left quadrant of the R, Q plane, it is (partially) destroyed in the upper right quadrant and there is weak vortex stretching in the $D = 0$ tail. The tail region is not well resolved on Fig.8 and the positive enstrophy production is confined to the narrow strip delineated by the zero contours. This strip becomes progressively more and more narrow as one looks at smaller scales, r , (which is why we limited our figures to rather large r/L), however, the existence of positive vortex stretching in the tail domain was verified analytically via the arguments presented later in this section (and in Appendix A). Next we compute the average strain skewness, $S_3 \equiv \int d\vec{\omega} \text{tr} \mathbf{s}^3 P_r(R, Q)$, which is the object associated with energy transfer [26], and find that it is strongly localized in the $D = 0$ Vieillefosse tail as shown in Fig.9. (Curiously, we find that in the elliptic region, $Q > 0$, the strain skewness changes sign three times - a fact that can be understood on the basis of the structure of the \mathbf{M} tensor given by (25).) Note that the energy transfer term in (9) is actually $\text{Tr} \mathbf{M}^2 \mathbf{M}^\dagger = \text{Tr} \mathbf{s}^3 - \frac{1}{4} \vec{\omega} \cdot \mathbf{s} \cdot \vec{\omega}$ so that vortex stretching also contributes to the energy flux. [58] Vortex stretching however does not dominate the energy transfer: while most of the enstrophy production is in the upper left quadrangle, Fig.8, the energy flux distribution $F(R, Q) \equiv -\alpha \int d\vec{\omega} \text{Tr} \mathbf{M}^2 \mathbf{M}^\dagger P_r(R, Q, \vec{\omega})$ is localized in the $D = 0$ tail where the negative $\text{Tr} \mathbf{s}^3$ lives, see Fig.10. Thus we arrive at the conclusion that from the energy transfer point of view, the active regions are dominated by the strain and not vorticity [12,25]. Also of interest is the appearance of distinct regions of weak *negative* energy transfer: e.g. the $R, Q > 0$ quadrangle where both σ and the energy flux are negative [44].

Remarkably, as seen from the comparison of Fig.7-10 and Figs. 11-14 the DNS exhibits a rather similar distribution of average enstrophy, enstrophy production and strain skewness in the Q, R plane. Both DNS and the model have positive enstrophy production in the upper left quadrant and in the $D = 0, R > 0$ tail, and negative σ in the upper right quadrangle; both have strain skewness strongly confined to the $D = 0, R > 0$ tail, and both exhibit the dominance of the strain skewness in the energy transfer. Furthermore, there is a clear correspondence of the positive and negative regions of $\text{tr} \mathbf{s}^3$ (Fig.9 and 13) and energy flux (Fig.10 and 14).

Much of this behavior can be understood by considering the "statistical geometry" of the flow (see Ashurst et al [8], Constantin [15] and Tsinober et al [25] for excellent discussions) and is inherited from the RE dynamics. Most of the vortex stretching occurs for $R < 0, Q > 0$ where the vorticity is aligned with the large positive eigenvector of the strain; this is immediately evident from the structure of the \mathbf{M} matrix at the saddle point controlling $\sigma(R, Q)$:

$$\mathbf{M}_\sigma = \begin{pmatrix} \lambda & \Delta & 0 \\ -\Delta & \lambda & 0 \\ 0 & 0 & -2\lambda \end{pmatrix} \quad (24)$$

where [59] $\lambda < 0$, since the off-diagonal elements of (24) define the vorticity along the direction with the strain

eigenvalue $-2\lambda > 0$. The tetrad dynamics then takes the \mathbf{M} field into the $R \approx 0$, $Q > 0$ region where λ and hence the stretching rate σ vanish before changing sign. The magnitude of vorticity reaches a maximum. In the peak vorticity region \mathbf{M} tensor has the form:

$$\mathbf{M}_e = \begin{pmatrix} \lambda & \Delta e^\gamma & 0 \\ -\Delta e^{-\gamma} & \lambda & 0 \\ 0 & 0 & -2\lambda \end{pmatrix} \quad (25)$$

with $\lambda \ll \Delta$ and $\gamma \ll 1$, so that the flow is essentially two dimensional with vorticity aligned with the nearly neutral strain direction.

The alignment of intense vorticity with the intermediate strain axis is well known [7,51,8,12,25] and its reappearance in the model is encouraging. The fate of the typical 2D vorticity is to implode under the action of the contracting strain (brought about by the low pressure of the vortex) [60]. The energy is transferred to larger scale.

To conclude we examine the geometry of \mathbf{M} in the $D = 0$ tail. Here the predominant \mathbf{M} configuration is

$$M_s = \begin{pmatrix} \lambda & 0 & \omega \\ 0 & \lambda & 0 \\ 0 & 0 & -2\lambda \end{pmatrix} \quad (26)$$

which leads to the strain eigenvalues

$$s_\alpha = \lambda; \quad s_\beta = \frac{3}{2}\lambda \sqrt{1 + \frac{\omega^2}{9\lambda^2}} - \frac{\lambda}{2} \quad (27)$$

and $s_\gamma = -s_\alpha - s_\beta$. The vorticity is aligned with the intermediate strain axis, which is stretching since the $s_\beta > 0$ consistent with the negative strain skewness $Tr \mathbf{s}^3 = 3s_\alpha s_\beta s_\gamma$. The normalized β -strain [8,39] $\left\langle \frac{s_\beta}{|\mathbf{s}|} |\lambda \right\rangle$ as a function of λ along the $D = 0$ line increases as $\left\langle \frac{\omega^2}{\lambda^2} |\lambda \right\rangle$ goes down with increasing λ as it is shown below in the Section and confirmed by Fig.15a,b for the DNS. To the extent that $P_r(R, Q)$ is peaked at $R = Q = 0$ and hence at $\lambda = 0$ the most probable configurations have $s_1 \gg s_2 \approx 0$ and are close to plane shear or 2D vorticity. Note that these most probable configurations have $Tr \mathbf{M}^2 \approx 0$ or $Tr \mathbf{s}^2 \approx \frac{1}{2}\bar{\omega}^2$ which means approximate *local* homogeneity - a much stronger statement than the homogeneity on average, i.e. $\langle Tr \mathbf{M}^2 \rangle = 0$! This must have serious implications for the pressure.

The exaggerated non-Gaussianity (i.e. Vieillefosse tail) of the deterministic model aside, there are also other qualitative differences between the results of the model and the DNS: e.g. the vorticity density in the DNS peaks at the origin and is skewed in the upper half plane, towards $R < 0$. This effect is even stronger for the vorticity distribution measured in the dissipative range: an asymmetry also visible in $P(R, Q)$ shown on Fig.3a. This can be understood as a result of enstrophy dissipation by viscosity which shifts the locus of null enstrophy growth and hence maximal enstrophy to configurations where of vorticity is still aligned with positive strain.

Let us further explore the results of the deterministic approximation. The exact solution on the $D = 0$ line (see Appendix A) exhibits strong asymmetry: even though the PDF is Gaussian along the $D = 0$ line both for $R > 0$ and $R < 0$, $\ln P(\lambda) \sim -\lambda^2(r/L)^{4(1-\alpha)h_\pm(\beta)}$ the characteristic exponents on the two sides are different, $h_+(\beta) > h_-(\beta)$. It is the h_- exponent which controls the behavior of low moments including the 3d and in order to impose constant energy flux we must require $(1-\alpha)h_-(\beta) = 2/3$ which forces K41 scaling on the "head" of the PDF in Fig.5a,b. The constant flux condition thus fixes a specific relation (determined in the Appendix A) between the model parameters: as β increases from 0 to $\approx .3$, α decreases from $1/3$ to 0.

However, while the scaling in the bulk of the PDF is K41, the scaling in the Vieillefosse tail is anomalous. Introducing rescaled variable $\tilde{\lambda} = \lambda r^{\frac{2}{3}}$, $\tilde{\Delta} = \Delta r^{\frac{2}{3}}$, and $\tilde{\omega} = \omega r^{\frac{2}{3}}$ we find that the $\tilde{\Delta}$ dependence of the action in the hyperbolic vicinity of the tail (which determines its width in the R, Q plane) has the asymptotic form:

$$S_+(\tilde{\lambda}, \tilde{\Delta}, \omega = 0) \sim \tilde{\lambda}^2 r^{2\gamma_+} + \tilde{\Delta}^2 r^{-2\eta} f_\Delta \left(\frac{\tilde{\Delta}}{\tilde{\lambda}} r^{-\eta-\gamma_+} \right) \quad (28)$$

where the scaling function $f_\Delta(0) = const$ and $f_\Delta(x) \sim x^\zeta$ for $x \gg 1$ with $\eta = \gamma_+ \zeta / (2 - \zeta)$. Similarly, the vorticity distribution on the $D = 0$ ($R > 0$) line is governed asymptotically by

$$S_+(\tilde{\lambda}, \tilde{\Delta} = 0, \tilde{\omega}) \sim \tilde{\lambda}^2 r^{2\gamma_+} + \tilde{\omega}^2 r^{-2\eta'} f_\omega \left(\frac{\tilde{\omega}}{\tilde{\lambda}} r^{-\eta'-\gamma_+} \right) \quad (29)$$

where $f_\omega(x) \sim x^\delta$ for $x \ll 1$ and $f_\omega(x) \sim x^{\delta-3}$ for $x \gg 1$ with $\eta' = \gamma_+(3-\delta)/(\delta-1)$. The anomalous exponents depend on β : $\gamma_+ \equiv 2(1-\alpha)(h_+(\beta) - h_-(\beta))$ varies from 0 at $\beta = 0$, ($\alpha = 1/3$) to $1/2$ at $\beta \approx .3$, $\alpha = 0$. Over the same range η varies from 1 to $3/2$. The exponents as a function of β are tabulated in the Appendix A

It follows that the conditional enstrophy in the Vieillefosse tail behaves for large λ as:

$$\langle \tilde{\omega}^2 | \tilde{\lambda} \rangle \sim (\tilde{\lambda})^{\frac{2\delta}{2+\delta}} r^{\frac{2\gamma_+\delta}{2+\delta} + 2\eta'} \quad (30)$$

implying an interesting non-trivial scaling relation between the strain and vorticity of the velocity gradient sheets associated with the high energy transfer regions.

We can also compute the contribution of the $D = 0$, $R > 0$ tail to the moments of the velocity gradient. E.g. we compute

$$\langle \tilde{\lambda}^n \rangle_{tail} = N \int d\tilde{\lambda}^3 \int d\tilde{\Delta}^2 \int d\tilde{\omega} \tilde{\lambda}^n e^{-S_+(\tilde{\lambda}r^{\gamma_+}, \tilde{\Delta}r^{-\eta}, \tilde{\omega}r^{-\eta'})} \sim r^{2\eta+3\eta'-(n+3)\gamma_+} \quad (31)$$

where the normalization factor $N \sim 1$ because it is dominated by the "head" of the PDF with K41 scaling, already factorized explicitly. Thus we conclude that the tail contribution is important only for sufficiently large n , when $n > n_c = (2\eta + 3\eta')/\gamma_+ - 3$ and the anomalous scaling becomes dominant over the normal contribution of the bulk of the PDF. We find that in the limit of $\beta \rightarrow 0$ and $\alpha \rightarrow 1/3$, $n_c \rightarrow \infty$ and the shape of the PDF, although non-Gaussian, becomes independent of the scale. This limit recovers the Kolmogorov 41 theory. The intermittency effect is maximized as $\beta \rightarrow .3$ and $\alpha \rightarrow 0$, where anomalous scaling appears for $n > 6$.

It is clear that although the PDF found in the present deterministic approximation of the model is on the whole far from Gaussian (imposed on integral scale) the approximation underestimates the intermittency effects. E.g. it predicts no deviations from K41 in the vorticity dominated $Q > 0$ region, in contrast to the DNS result which in that region exhibits r -dependence associated with the development of an exponential (or sub-exponential) tail on smaller scales. It is equally clear that the description of such a tail is beyond the currently employed approximation. After all, the asymptotic behavior of the PDF, i.e. the statistics of large fluctuations, is dominated by fluctuations. One does however expect to find the exponential asymptotics [41] once the fluctuations are accounted for via a proper semi-classical calculation. There thus appears to be two mechanisms contributing to the intermittency: 1) the deterministic non-linear interactions in the energy transfer region as indicated by our present calculation and 2) the effect of small scale fluctuations responsible for the exponential asymptotics of the PDF. The latter mechanism is analogous to the one responsible for the intermittency of the Passive Scalar [16,20,19,18].

VI. CONCLUSIONS.

In the preceding Sections we have introduced and began to analyze the phenomenological model of inertial scale velocity fluctuations defined through the velocity gradient tensor coarse-grained over a region specified by a tetrad of points. The dynamics of this field was decomposed into the non-linear deterministic component representing local same-scale interactions and a Gaussian stochastic component with embedded K41 scaling representing interactions non-local in space and the incoherent contribution of the velocity fluctuations from scales smaller than that of the tetrad. The deterministic component is closely related to the RE dynamics of Vieillefosse [33] model. The latter, although marred by the unphysical finite time singularity, [61] has been an appealing candidate description for the dynamics of the local velocity gradient [8,10,39]. A novel aspect of our model is the elevation of the velocity gradient dynamics to the coarse-grained level and the introduction of the tetrad tensor (ρ) dynamics which explicitly introduces the scale and the measure of anisotropy generated through the strain induced distortion of the Lagrangian volume. This allows to construct an anisotropic model of the coarse grained pressure Hessian which eliminates the finite time singularity from the deterministic dynamics by suppressing the work done by the pressure on the distorted fluid element. Furthermore, the explicit appearance of the current scale allows to build in K41 spectrum in the stochastic component [67] of the dynamics. An important reason for working with the coarse grained field is that in the dynamics of the purely inertial range fields the direct contribution of the viscosity can be neglected [69]. Instead, the ultimately viscous dissipation is incorporated through the effect of the incoherent small scales acting through the eddy damping $D_{nl} + D_\perp$ terms in the model. The deterministic dynamics plays the key role in transferring energy down scale. This transfer occurs due to the volume preserving distortion of the fluid element which leads to the reduction of at least one of its principle axis.

Our heuristic derivation of the model was fortified by the numerical test of (3a) through the construction of the conditional flow for the invariants of \mathbf{M} . The deterministic part of (3a) appears to be quite close to the conditional flow at least for isotropic tetrads $\rho = \mathbf{1} r$. It will be important to extend the numerical study to anisotropic ρ and to

find a way of examining the stochastic contribution to the dynamics. The validity of the local approximation of the pressure Hessian [10] and the neglect of non-local correlations remain the key issues.

The tetrad model respects K41 scaling ($\mathbf{M} \rightarrow b\mathbf{M}$, $\rho \rightarrow b^{-3/2}\rho$), both on the operator (7) and the integral scale boundary condition (16) levels. Yet, as illustrated by our crude deterministic approximation the resulting PDF has non-trivial, model parameter dependent anomalous scaling. The Kolmogorov scaling has to be re-imposed on the level of the 3d moment by choosing the parameters so as to make the energy flux scale independent. Except for one particular limit ($\beta \rightarrow 0$, $\alpha \rightarrow 1/3$) where the PDF has K41 behavior, high moments exhibit anomalous scaling. Remarkably, while this anomalous scaling has little to do with the Kolmogorov-Obukhov arguments [26,1] it does originate in the domain of energy transfer: the Vieillefosse tail.

The deterministic approximation employed in Section 5 grossly overestimates the extent of the Vieillefosse tail in $P(Q, R)$ but it does bear resemblance to the PDF observed in the DNS. It also generates plausible distributions of enstrophy, enstrophy production and strain skewness. The present analysis provides a clear dissection of the high enstrophy and the high enstrophy production regions, identifies the difference in the vorticity-strain alignment in the two regions [25] and exhibits their dynamical connection. As explained in Section 3, much of this sensible phenomenology was inherited from the RE dynamics [8]. The elimination of the Vieillefosse finite time singularity was however essential in order to have a model with stationary statistics.

The energy transfer for isotropic ρ configurations occurs via non-linear eddy damping [46,39] $tr\mathbf{M}^2\mathbf{M}^\dagger$ term (9), which combines contributions of strain skewness and vortex stretching. Within our present crude deterministic approximation, the energy transfer occurs largely in the Vieillefosse tail and is due to large negative trs^3 . In this region strain has two positive eigenvalues and Lagrangian volumes are deformed into pancakes or ribbons, i.e. this is the region of sheet formation [50]. In contrast, the vortex filaments are generated in the $Q > 0$, $R < 0$ quadrant where enstrophy production is peaked. This region does not contribute as much to the energy flux. Furthermore, the maximal vorticity region is characterized by nearly 2D configurations and does not contribute at all - a notion consistent with recent numerical results [12]. Yet, whereas we are optimistic about correct description of the high $-trs^3$ tail in the model, the correct description of the high σ region may be more difficult because of the importance of long-range strain in vortex stretching.

In order to enable a more quantitative comparison of the model and the DNS the treatment of the model must include the effect of the fluctuations which control the asymptotic behavior of the PDF. Our present, deterministic, approximation overestimates the PDF in the narrow Vieillefosse tail, while underestimating the asymptotic behavior of the PDF elsewhere in the Q, R plane. Both effects are due to the neglect of the fluctuations. Since the relevant Fokker-Planck equation lives in the $d^2 - 1 + d(d+1)/2 = 14$ dimensional \mathbf{M}, ρ space the direct numerical approach seems out of question. However one may hope to make progress with the semi-classical analysis of the path integral representation (20) along the lines of [41,53]. This approach is valid for the calculation of the PDF tails and associated anomalous scaling. We expect that the fluctuation effects will change the Gaussian decay of the PDF tails found in the deterministic approximation to the exponential, [70] e.g.: $\lambda^{-a} e^{-c\lambda r^b}$.

An interesting simplification appears in the limit of strong transverse diffusion $C_\perp \gg 1$ which corresponds to the physically sensible regime of strong re-isotropisation of the tetrads arising from the action of incoherent small scale fluctuations. In that limit the PDF becomes nearly uniform over the $\rho^2 = const$ shells and can be projected onto the s and d representations of $SO(9)$ acting on ρ_i^a :

$$P(\mathbf{M}, \rho) \approx \Psi(\mathbf{M}, \rho^2) + \frac{1}{2d^2 C_\perp} (\rho_i^a \rho_j^b - \frac{1}{d^2} \rho^2 \delta^{ab} \delta_{ij}) \Phi_{ij}^{ab}(\mathbf{M}, \rho^2). \quad (32)$$

Curiously, this nearly isotropic approximation doubles as a $d \gg 1$ expansion [28,19,29] because the d -wave mode of $SO(d^2)$ is suppressed by the $l(l+d^2-2)$ total angular momentum factor with $l=2$. This expansion allows a considerable simplification of (7) and (20).

Several related models are worth mentioning. The present model appears to be the real space, Lagrangian counterpart of the momentum space, Eulerian "shell" model proposed by Siggia [72]. Yet, the geometrical and statistical implications of that model have not been fully explored and we do not at present understand the relative merits of the assumptions involved in the two models. The logic which led to (3a,3b) can and has been applied to the Passive scalar problem, in which case one would replace \mathbf{M} by a Gaussian random field. This would lead to a PS model of the type considered in [20,73] closely related to the Kraichnan's [24] model. It would be interesting also to explore whether the 2D version of (3a,3b) could provide a sensible description of 2D turbulence where the physics is very different. In that case the deterministic left hand side of (3a) would vanish for isotropic "triads". We do not presently know if the model can generate the inverse cascade. Finally, if the tetrad model provides a reasonable description of turbulent fluctuations in the homogeneous case, it will be interesting to attempt to generalize it to the inhomogeneous and anisotropic case: e.g. one could study the statistics of tetrads moving away from the wall in the boundary layer.

Last but not least, two remarks concerning the relation with the experiment. The traditional approach to turbulence and most of the existing data involves velocity difference at two points. This two point statistics can be extracted

from the tetrad statistics by averaging over "unobserved" variables $P(\vec{v}, \vec{\rho}_1) = \int d\vec{\rho}_2 \int d\vec{\rho}_3 \int d\mathbf{M} \delta(\rho_1^a M_{ab} - v_b) P(\mathbf{M}, \rho)$. Conversely, it would be very interesting to study tetrad statistics experimentally. For that we need a velocity measurement at 4 points in the inertial range, which can be obtained from 3 (crossed wire) probes (say a fixed probe at the origin and two movable probes at $(x, y, z) = (0, \sqrt{3/2}r, \pm 1/2r)$ in a flow with $\langle v_x \rangle \neq 0$). The time lag (on the static probe) then can be used to provide the 4th measurement [74,75]. The PDF coarse grained velocity gradient may then be obtained. Quite independently of the predictions of the present model, the (R, Q) -plane density of the 2nd and 3d order invariants (e.g. Figs. 8-14) are quite illuminating in dissecting the role of vorticity and strain in intermittency and the possible difference in their anomalous scaling.

We conclude finally that despite its relative simplicity the tetrad model is surprisingly rich in physics, offering an insight both into the geometry and dynamics as well as the statistical and scaling properties of the inertial range fields. Many non-trivial statistical objects can be calculated in terms of the 3 parameters of the present model. Further work and detailed comparison with the DNS and the experiment will establish the degree of success and failure of this model.

VII. ACKNOWLEDGEMENTS

It is a pleasure to thank A. Libchaber, E.D. Siggia and A. Tsinober for stimulating discussions. MC acknowledges support of the R.H. Dicke fellowship and the hospitality of Bell Labs. We also greatly acknowledge the grant of computer time from IDRIS (France).

APPENDIX A: SCALING IN THE DETERMINISTIC LIMIT

Consider Lagrangian dynamics of \hat{M} and \hat{g} described by (21a,21b) for the following class of matrices forming a subspace in the Elliptic region ($D \geq 0$)

$$\hat{M} = \begin{pmatrix} \lambda & \Delta & 0 \\ -\Delta & \lambda & 0 \\ 0 & 0 & -2\lambda \end{pmatrix}, \quad \hat{g} = \begin{pmatrix} x & 0 & 0 \\ 0 & x & 0 \\ 0 & 0 & y \end{pmatrix}. \quad (\text{A1})$$

We arrive at the system of equations

$$\frac{d \ln [\lambda]}{\lambda dt} = (1 - \alpha) \frac{z - 4 - \mu^2 z}{z + 2}, \quad (\text{A2})$$

$$\frac{d \ln [\mu]}{\lambda dt} = (1 - \alpha) \frac{z + 8 + \mu^2}{z + 2}, \quad (\text{A3})$$

$$\frac{dz}{\lambda dt} = -6z + \text{sgn}[\lambda] \frac{\beta}{3} \sqrt{6 + 2\mu^2} (1 + 2z)(1 - z), \quad (\text{A4})$$

$$\frac{d \ln [G]}{\lambda dt} = \frac{4(1 - z)}{1 + 2z}, \quad (\text{A5})$$

with $\mu \equiv \Delta/\lambda$, $z \equiv x/y$ ($z(0) = 1$), $G \equiv \text{tr}[\hat{g}] = 2x + y$. This system is integrable in quadratures if either $\beta = 0$ or $\Delta(0) = 0$ (and therefore, $\Delta(t) = 0$, for any other t). We shall now calculate the effective action $S \equiv -\ln[P(\mathbf{M}, \mathbf{g})]$ (see (22)) for these two cases.

1. Elliptic region, $\beta = 0$.

Integration of the system (A2-A5) gives

$$\lambda'^2 = \left[\frac{3x'^2 r^2}{x'^3 + 2r^6} \right]^{1-\alpha} \quad (\text{A6})$$

$$\times \left(\lambda^2 - \Delta^2 3^{\alpha-1} \left[\left(\frac{r^2}{x'} \right)^{1-\alpha} {}_2F_1 \left(\frac{1-\alpha}{3}, \alpha, \frac{4-\alpha}{3}, \frac{-2r^6}{x'^3} \right) - {}_2F_1 \left(\frac{1-\alpha}{3}, \alpha, \frac{4-\alpha}{3}, -2 \right) \right] \right),$$

$$\Delta' = \Delta \left(\frac{r^2}{x'} \right)^{1-\alpha}, \quad y' = \frac{r^6}{x'^2}, \quad (\text{A7})$$

where the $''$ notation stands to mark the $(-T)$ preimage. These expressions allow to rewrite the effective action in terms of r, λ and Δ , providing T is fixed by $tr[\hat{\rho}(-T)\hat{\rho}(-T)^+] = 2x' + r^6/x'^2 = 3L^2 = 3$. There are two solutions for x' realized separately depending on the sign of λ' .

First, consider the region with λ being positive during the all Lagrangian evolution. At $r \ll 1$, the respective value of the effective action is

$$\lambda' > 0, \quad S \rightarrow 3\lambda^2 \left(\frac{r^2}{2}\right)^{1-\alpha} + \Delta^2 \left(\frac{\sqrt{3}}{r}\right)^{2(1-\alpha)}. \quad (\text{A8})$$

We find that the action becomes infinite at $r \rightarrow 0$ in the domain.

If $\lambda(t)$ is negative (at least at the final stage of the backward in time evolution) and $r \ll 1$ the effective action is

$$\lambda' < 0, \quad S \rightarrow 3 \left[\lambda^2 + \Delta^2 3^{\alpha-1} {}_2F_1 \left(\frac{1-\alpha}{3}, \alpha, \frac{4-\alpha}{3}, -2 \right) \right] \left(\frac{3r^2}{2} \right)^{1-\alpha}. \quad (\text{A9})$$

The transition region between (A8) and (A9) shrinks with $r \rightarrow 0$. The crossover occurs at the intersection of the $\lambda = \mu\Delta$ line in the λ, Δ (Q, R) plane. μ , depends on both α and r and has the following asymptotic form:

$$\mu|_{r \rightarrow 0} \rightarrow \begin{cases} 3^{\alpha-1} [2^{[\alpha-1]/3} \Gamma(\frac{4-\alpha}{3}) \Gamma(\frac{4\alpha-1}{3}) / [-3\Gamma(\alpha-1)] {}_2F_1(\frac{1-\alpha}{3}, \alpha, \frac{4-\alpha}{3}, -2)], & \alpha > 1/4; \\ 3^{1/2-\alpha} (1-\alpha) r^{4\alpha-1} / [2^{\alpha+1} (1-4\alpha)(2\alpha+1)], & \alpha < 1/4. \end{cases} \quad (\text{A10})$$

Therefore, a sector in the right part of Q, R plane bounded by the $D = 0$ line from below and the $\lambda = \mu\Delta$ one from above forms a low probability gulf of the PDF.

2. Zero discriminant line: $D = 0$.

For the $\delta = D = 0$ line, the integration of (A2-A5) yields

$$\begin{aligned} \ln \left[\frac{G'}{3r^2} \right] &= 4 \int_{z'}^1 \frac{(1-\tilde{z})d\tilde{z}}{\left[6\tilde{z} - \beta(1+2\tilde{z})(1-\tilde{z}) \sqrt{2/3} \text{sgn}[\lambda] \right] (1+2\tilde{z})}, \\ \ln \left[\frac{\lambda}{\lambda'} \right] &= (1-\alpha) \int_{z'}^1 \frac{(4-\tilde{z})d\tilde{z}}{\left(6\tilde{z} - \beta(1+2\tilde{z})(1-\tilde{z}) \sqrt{2/3} \text{sgn}[\lambda] \right) (2+\tilde{z})}. \end{aligned} \quad (\text{A11})$$

The dynamics (on $D = 0$ line) does not change the sign of λ so that $\text{sgn}[\lambda]$ is constant.

For positive λ , $\lambda(t)$ is monotonically decreasing while $G(t)$ grows and $z(t)$ decreases. For small enough initial $G(=3r^2 \ll 1)$, z approaches z_+ ,

$$z_+ \equiv \frac{\beta - 3\sqrt{6} + \sqrt{54 - 6\beta\sqrt{6} + 9\beta^2}}{4\beta}. \quad (\text{A12})$$

For z' close to z_+ one finds

$$\frac{\lambda'}{\lambda} \rightarrow \text{const} * [z' - z_+]^{C_1^+(1-\alpha)}, \quad G' \rightarrow \frac{\text{const} * r^2}{[z' - z_+]^{C_2^+}}, \quad (\text{A13})$$

where

$$C_1^+ = \sqrt{3/2} \frac{4 - z_+}{(2 + z_+) \sqrt{54 - 6\beta\sqrt{6} + 9\beta^2}}, \quad (\text{A14})$$

$$C_2^+ = \sqrt{24} \frac{1 - z_+}{(1 + 2z_+) \sqrt{54 - 6\beta\sqrt{6} + 9\beta^2}}. \quad (\text{A15})$$

We get the following asymptotic behavior for the effective action for $D = 0$ and $R, \lambda > 0$:

$$S \sim \lambda_L^2 \sim \lambda^2 r^{4(1-\alpha)h_+}, \quad (\text{A16})$$

with $h_+ \equiv C_1^+/C_2^+$.

If λ is negative, $\lambda(t)$ increases in absolute value while $z(t)$ decreases at the initial stage of backward in time evolution. The dynamics changes (r is supposed to be very small) once z crosses 4 and $\lambda(t)$ starts moving towards the origin. z keeps growing to approach z_- ,

$$z_- = \frac{3\sqrt{6} + \beta + \sqrt{54 + 6\sqrt{6}\beta + 9\beta^2}}{4\beta}. \quad (\text{A17})$$

For z close to z_- one finds

$$\left| \frac{\lambda'}{\lambda} \right| \rightarrow \text{const} * [z' - z_-]^{C_1^-(1-\alpha)}, \quad G' \rightarrow \frac{\text{const} * r^2}{[z' - z_-]^{C_2^-}}, \quad (\text{A18})$$

where

$$C_1^- = \sqrt{3/2} \frac{z_- - 4}{(2 + z_-)\sqrt{54 + 6\sqrt{6}\beta + 9\beta^2}}, \quad (\text{A19})$$

$$C_2^- = \sqrt{24} \frac{z_- - 1}{(1 + 2z_-)\sqrt{54 + 6\sqrt{6}\beta + 9\beta^2}}. \quad (\text{A20})$$

Finally, we get the following asymptotic behavior for the effective action for $D = 0$ and $R, \lambda < 0$:

$$S \sim \lambda_L^2 \sim \lambda^2 r^{4(1-\alpha)h_-} \quad (\text{A21})$$

with $h_- \equiv C_1^-/C_2^-$. Note, that $h_- \leq h_+$.

Remarkably, the numerical study of the action shows that this scaling found analytically for the $D = 0, R < 0$ line holds everywhere in the Q, R plane except for the Vieillefosse tail, $D = 0, R > 0$. Hence the main body of the PDF, which determines the low moments, scales according to (A21). In order to impose constant energy flux we fix the scaling of the low moments (including the 3d) to the K41 value, which requires

$$\alpha = 1 - \frac{1}{3h_-}, \quad (\text{A22})$$

thus relating α and β parameters of the model. α decreases with β increase from $1/3$ at $\beta = 0$ (an exceptional case when tail and the body of the PDF scale the same way) to 0 at $\beta \approx 0.3$. We keep β as free parameter in the interval $[0, \approx 0.3]$ and calculate the respective values of other exponents numerically Table 1.

- [1] U. Frisch, *Turbulence : the legacy of AN Kolmogorov*, Cambridge University Press, Cambridge (1995);
- [2] K. Sreenivasan, R.A. Antonia, 'The Phenomenology of Small Scale Turbulence', Ann. Review of Fluid Mech, (1997).
- [3] R. A. Antonia and C. W. van Atta, J Fluid Mech, **84**, 561-580. (1978).
- [4] P. Tabeling, G. Zocchi, F. Belin, J. Maurer, and H. Willaime, 'Probability density function, skewness and flatness in large Reynolds number turbulence', Phys. Rev. E **55**, 1613-1621, (1994).
- [5] M. Nelkin, 'In what sense is turbulence an unsolved problem?', Science **255**, 566 (1992).
- [6] R.H. Kraichnan, 'Models of Intermittency in Turbulence', Phys. Rev. Lett., **65**, 575-579, (1990).
- [7] E. Siggia, 'Numerical Study of Intermittency in 3-D Turbulence', J. Fluid Mech, **107**, 375-406 (1981).
- [8] W. Ashurst, A. Kerstein, R. Kerr and C. Gibson, 'Alignment of Vorticity and Scalar Gradient with Strain rate in Simulated Navier-Stokes Turbulence', Phys. Fluids, **30**, 2343-2353 (1987).
- [9] S. Douady, Y. Couder and M.E. Brachet, 'Direct observation of Intense Vortex Filaments in Turbulence', Phys. Rev.Lett. **67**, 983-986 (1991).
- [10] Z.-S. She, E. Jackson and S. Orszag, 'Structure and Dynamics of Homogeneous Turbulence: Models and Simulations', Proc. R. Soc. Lond., **434**, 101-124, (1991).
- [11] A. Vincent and M. Meneguzzi, 'The Spatial Structure and Statistical Properties of Homogeneous Turbulence', J. Fluid Mech **225**, 1-25, 1991.

- [12] J. Jimenez, A. Wray, P. Saffman and R. Rogallo, 'The structure of Intense Vorticity in Homogeneous Isotropic Turbulence', *J. Fluid Mech.*, **255**, 65-91, (1993).
- [13] J. Jimenez, 'Kinematic Alignment Effects in Turbulent Flows', *Phys. Fluids* **A 4**, 652-654, (1992).
- [14] A. Tsinober, E. Kit and T. Dracos, 'Experimental Investigation of the Field of Velocity Gradients in Turbulent Flows', *J. Fluid Mech.*, **242**, 169-192, (1992).
- [15] P. Constantin, 'Geometrical Statistics In Turbulence', *SIAM Rev.* **36**, 73, (1994).
- [16] R. H. Kraichnan, 'Anomalous Scaling of a Randomly Advected Passive Scalar', *Phys. Rev. Lett.* **72**, 1016 (1994).
- [17] R.H. Kraichnan, V. Yakhot and S. Chen, 'Scaling relations for a randomly advected passive scalar field', *Phys. Rev. Lett.* **75**, 240 (1995).
- [18] K. Gawędzki and A. Kupiainen, 'Anomalous scaling of the passive scalar', *Phys. Rev. Lett.* **75**, 3834 (1995).
- [19] M. Chertkov, G. Falkovich, I. Kolokolov, and V. Lebedev, 'Normal and anomalous scaling of the fourth-order correlation function of randomly advected passive scalar', *Phys. Rev. E* **52**, 4924 (1995).
- [20] B. I. Shraiman and E. D. Siggia, 'Anomalous scaling of a passive scalar in a turbulent flow', *C. R. Acad. Sci.* **321**, 279 (1995).
- [21] A. Polyakov, 'Turbulence without pressure', *Phys. Rev. E* **52**, 6183 (1995).
- [22] W. E, K. Khanin, A. Mazel, and Y. Sinai, 'Probability distribution for the random forced Burgers equation', *Phys. Rev. Lett.* **78**, 1904 (1996).
- [23] J. P. Boucheau, M. Mezard, G. Parisi, 'Scaling and intermittency in Burgers turbulence', *Phys. Rev. E* **52**, 3656 (1995).
- [24] R. H. Kraichnan, 'Small-Scale Structure of a Scalar Field Convected by Turbulence', *Phys. Fluids* **11**, 945 (1968); and 'Convection of a passive scalar by a quasi-uniform random straining field', *J. Fluid Mech.*, **64**, 737 (1974).
- [25] A. Tsinober, L. Shtilman and H. Vaisburd, 'A study of properties of Vortex Stretching and Enstrophy Generation in Numerical and Laboratory Turbulence', *Fluid Dynamics Research*, **21**, 477-494, (1997); and A. Tsinober, 'Is concentrated vorticity that important?', *Eur. J. Mech., B Fluids*, **17**, 421-449, (1998).
- [26] A.S. Monin and A.M. Yaglom, *Statistical Fluid Mechanics*, MIT Press, (1975).
- [27] This expectation follows from examining the exact expression for the pressure Hessian in terms of the integral over $tr(\partial v)^2$ and observing that upon coarse-graining over region of size R it reduces approximately to a sum over many uncorrelated volumes (of size R). For large "d" the number of uncorrelated R-volumes in a shell surrounding the central - local - region is large.
- [28] J-D. Fournier, U. Frisch and H. Rose, 'Infinite-Dimensional Turbulence' *J. Phys.* **A**, **11**, 187-198 (1978).
- [29] V. Yakhot, 'Strong turbulence in D-dimensions', *chao-dyn*/9805027.
- [30] S. Pope, 'Lagrangian PDF Methods for Turbulent Flow', *Ann. Rev. of Fluid Mech.*, **26**, 23, (1994).
- [31] W.C. Reynolds and S.C. Kassinos, 'A One-Point model for the Evolution of Reynolds Stress and Structure Tensors in Rapidly Deformed Homogeneous Turbulence', *Proc. R. Soc. London* **A 451**, 87, (1995).
- [32] P.R. van Slooten and S.B. Pope, 'PDF Modeling for Inhomogeneous Turbulence with Exact Representation of Rapid Distortions', *Phys. Fluids*, **9**, 1085, (1997).
- [33] P. Vieillefosse, 'Internal Motion of a Small Element of a Fluid In inviscid Flow', *Physica* **125A**, 150-162, (1984).
- [34] J. Léorat, Thèse de Doctorat, Université Paris-VII (1975).
- [35] B.J. Cantwell, 'Exact Solution of a Restricted Euler Equation for the Velocity Gradient Tensor' *Phys. Fluids*, **A 4**, 782-793, (1992).
- [36] B. Cantwell, 'On the Behavior of the velocity Gradient Tensor Invariants in DNS of Turbulence', *Phys. Fluids*, **A 5**, 2008-2013, (1993).
- [37] H. Blackburn, N. Mansour and B. Cantwell, 'Topology of Fine-Scale Motions in Turbulent Channel Flow', *J. Fluid Mech.*, **310**, 269-292, (1996).
- [38] The relation of pressure anisotropy $\Pi_{a,b}$ to the shape of the tetrad given by (3c) is presented here as a model assumption. Alternatively, one could start with the pressure anisotropy tensor (defined over spherical volume of size R) and study its Lagrangian dynamics which, if the present assumption is correct, should be consistent with (3b,c).
- [39] V. Borue and S. A. Orszag, 'Local energy flux and subgrid scale statistics in three-dimensional turbulence', *J. Fluid Mech.* **336**, 1 (1998).
- [40] The Lagrangian path representation also allows incorporation of viscosity (in analogy with scalar diffusivity [41]) via addition of a Langevin noise source in (3b) or equivalently an additional $\nu \delta_{a,b} \delta_{i,j} \delta(t)$ term in (5b). It however plays no role as long as one works with pure inertial range, coarse grained quantities.
- [41] B. I. Shraiman and E. D. Siggia, 'Lagrangian path integrals and fluctuations in random flow', *Phys. Rev. E* **E49**, 2912 (1994).
- [42] The latter holds if $\langle \mathbf{M} \rangle \equiv \int d\mathbf{M} \mathbf{M} P(\mathbf{M}, \rho) = 0$. Note also other physical constraints due to homogeneity, e.g. $\langle tr \mathbf{M}^2 \rangle = \langle tr \mathbf{M}^3 \rangle = 0$ in the limit $Tr(\rho \rho^\dagger) \rightarrow 0$.
- [43] L. D. Landau and E.M. Lifshitz, 'Fluid Mechanics', Pergamon Press, (1960).
- [44] W. Reynolds, 'The Potential and the Limitations of Direct and Large Eddy Simulation', in *Whither Turbulence ?* ed. J.L. Lumley, p.313, Springer (1990).
- [45] C.M. Meneveau, in *Whither Turbulence ?* ed. J.L. Lumley, p.313, Springer (1990).
- [46] J. Bardina, J. Ferziger and W. Reynolds, 'Improved Subgrid Scale Models for Large Eddy Simulation', AIAA Paper

- 80-1357, (1980).
- [47] This sort of singular solutions have been earlier noted by others (e.g. Childress and Siggia - private communications).
 - [48] We have already seen that the introduction of the Π tensor also eliminates the unphysical contribution of the local pressure to $\partial_t V^2$ which underlies the singularity [33].
 - [49] By ribbon we mean configuration with two unequal stretching directions.
 - [50] A. Betchov, 'An inequality concerning the production of vorticity in isotropic turbulence', J. Fluid Mech. **1**, 497-504, 1956.
 - [51] R. M. Kerr, 'Higher order derivative correlations and alignment of small scale structures in isotropic turbulence', *J. Fluid Mech* **153**, 31 (1985).
 - [52] For simplicity we shall for the time being ignore the physical constraint imposed on the PDF by the homogeneity $\langle \text{tr} \mathbf{M}^2 \rangle = 0$. It can be easily added.
 - [53] M. Chertkov, 'Instanton for random advection', Phys. Rev. E **55**, 2722 (1997).
 - [54] G. Falkovich, I. Kolokolov, V. Lebedev, and A. Migdal, 'Instantons and Intermittency', Phys. Rev. E **54**, 4896 (1996).
 - [55] Z.-S. She, E. Jackson and S. Orszag, 'Intermittent Vortex Structures in Homogeneous and Isotropic Turbulence' Nature, **344**, 226-228, (1990)
 - [56] This is not an essential approximation and proper integration may be performed numerically.
 - [57] W. Press, S. Teukolsky, W. Vetterling, and B. Flannery, *Numerical Recipes in Fortran*, Cambridge U. Press, (1992)
 - [58] Homogeneity, restored at $r \rightarrow 0$, dictates [26] $\langle \text{Tr} \mathbf{M}^3 \rangle = \langle \text{Tr} \mathbf{s}^3 \rangle + \frac{3}{4} \langle \vec{\omega} \cdot \mathbf{s} \cdot \vec{\omega} \rangle = 0$ which allows to relate average energy flux to the average enstrophy production.
 - [59] The degree of alignment of course would vary if conditioned on σ or e as an independent variable.
 - [60] As the trajectory enters the $\sigma < 0$ upper right quadrangle: $\begin{pmatrix} 0 & \omega & 0 \\ -\omega & 0 & 0 \\ 0 & 0 & 0 \end{pmatrix} \rightarrow \begin{pmatrix} dt\omega^2 & \omega & 0 \\ -\omega & dt\omega^2 & 0 \\ 0 & 0 & -2dt\omega^2 \end{pmatrix}$ for isotropic tetrad.
 - [61] While the question of existence of finite times singularities is still being debated, it is clear that it has to be generated by some non-local effect, rather than by local stretching effect [62–66].
 - [62] A. Pumir and E. D. Siggia, 'Collapsing solutions to the 3-D Euler equations', Phys. Fluids **A2**, 220 (1990).
 - [63] A. Pumir and E. D. Siggia, 'Development of singular solutions to the axisymmetric Euler equations', Phys. Fluids **A4**, 1472 (1992).
 - [64] R. M. Kerr, 'Evidence for a singularity of the three-dimensional incompressible Euler equations', Phys. Fluids **A5**, 1725 (1993).
 - [65] R. B. Pelz and Y. Gulak, 'Evidence for a real time singularity in hydrodynamics from time series analysis', Phys. Rev. Lett. **79**, 4998 (1997).
 - [66] R. Grauer, C. Mariani and K. Germaschewski, 'Adaptive mesh refinement for singular solutions of the incompressible Euler equations', Phys. Rev. Lett **80**, 4177 (1998).
 - [67] An earlier effort to construct a stochastic generalization of RE dealt with only local gradients and resulted in a very different type of model. [68]
 - [68] S. Ghirimaghi and S. Pope, 'A diffusion model for velocity gradients in turbulence', Phys. Fluids **A 2**, 242 (1990).
 - [69] By comparison, the two-point closures of Kraichnan [16] and Polyakov [21] require an ansatz for the evaluation of the $\langle v(r)^m \nu \Delta v(r) \rangle$ "anomaly" contribution.
 - [70] Note that the "tails" here refer to the intermediate asymptotics where λ is much larger than its r.m.s. value but smaller than the characteristic large scale velocity over r . The latter condition is imposed by the bound on velocity difference PDF imposed by the single point PDF [71].
 - [71] A. Noullez, G. Wallace, W. Lempert, R.B. Miles and U. Frisch, 'Transverse velocity increments in turbulent flow using the RELIEF technique,' J. Fluid Mech, **339**, 287, (1997).
 - [72] E.D. Siggia, 'Model of intermittency in three dimensional turbulence,' Phys. Rev. **A 17**, 1166-1176 (1978).
 - [73] B. I. Shraiman and E. D. Siggia, 'Symmetry and scaling of turbulent mixing', Phys. Rev. Lett. **77**, 2463, (1996) and 'Anomalous scaling of passive scalar near Batchelor limit', Phys. Rev. **E 57**, 2965 (1998).
 - [74] L. Mydlarsky, A. Pumir, B. I. Shraiman E. D. Siggia, and Z. Warhaft, 'Structure and Multi-point Correlators for Turbulent Advection', Phys. Rev. Letters, **81**, 4373, (1998).
 - [75] L. Mydlarsky and Z. Warhaft, 'Multi-point Correlators for Turbulent Advection', Phys. Fluids, to appear (1998).

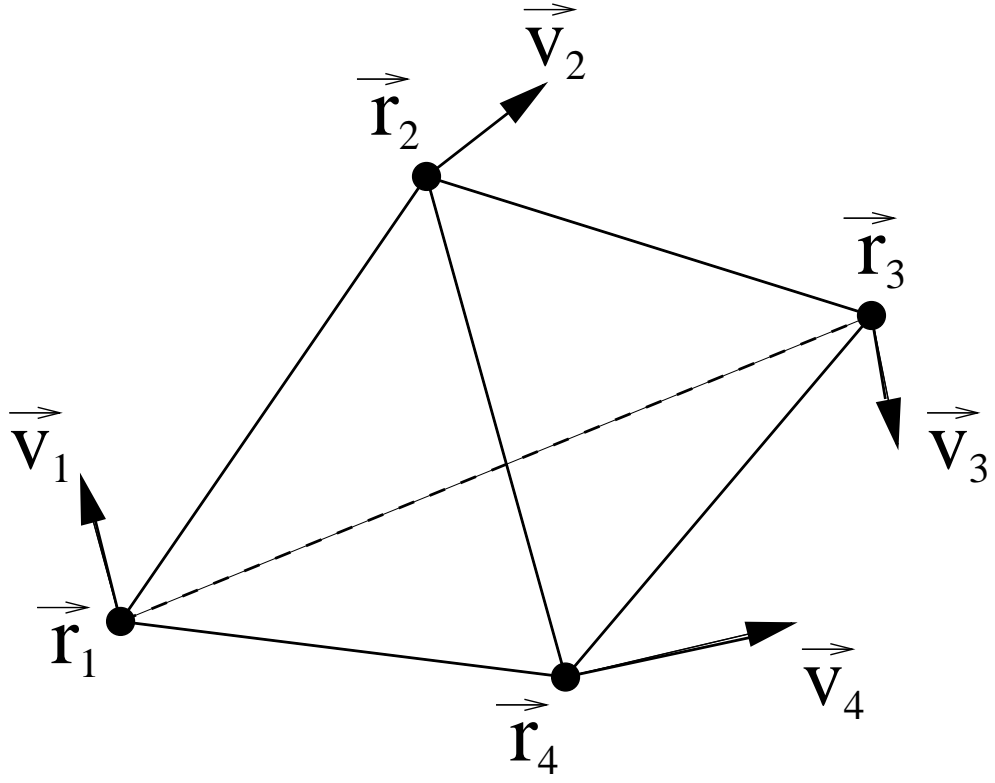


FIG. 1. Four Lagrangian points forming a "tetrad". The velocities at the four points define the coarse grained velocity gradient field.

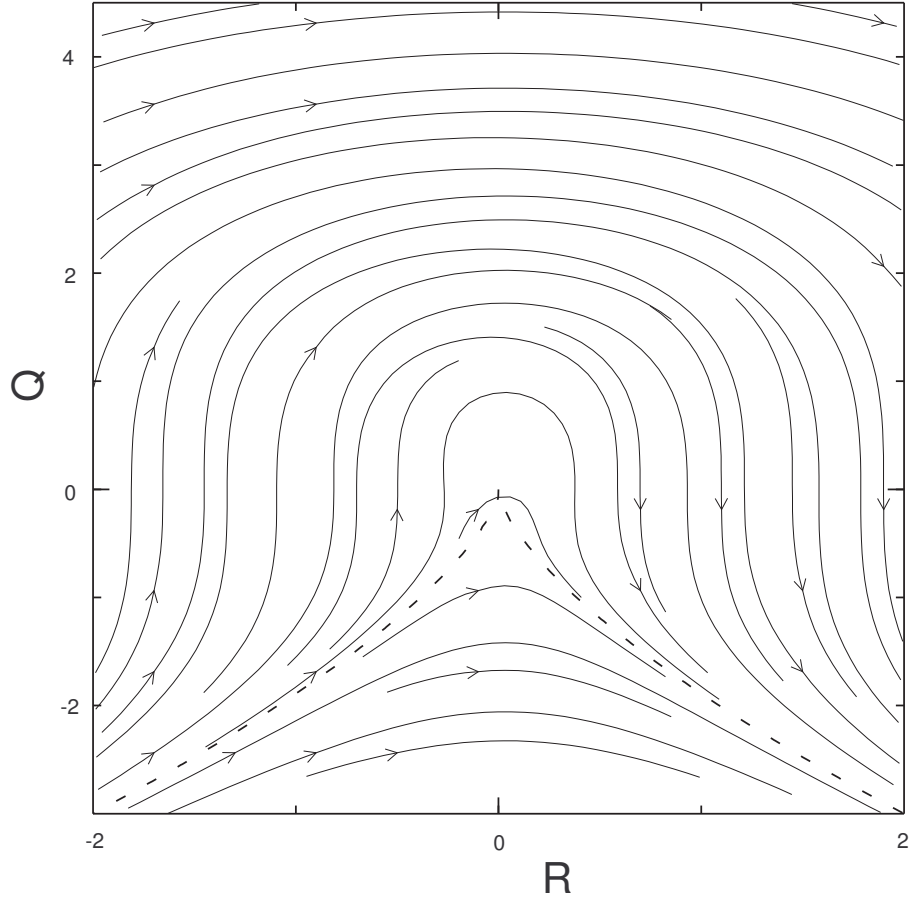


FIG. 2. The Restricted Euler flow of velocity gradient invariants $Q = -\frac{1}{2}\text{tr}\mathbf{M}^2$ and $R = -\frac{1}{3}\text{tr}\mathbf{M}^3$.

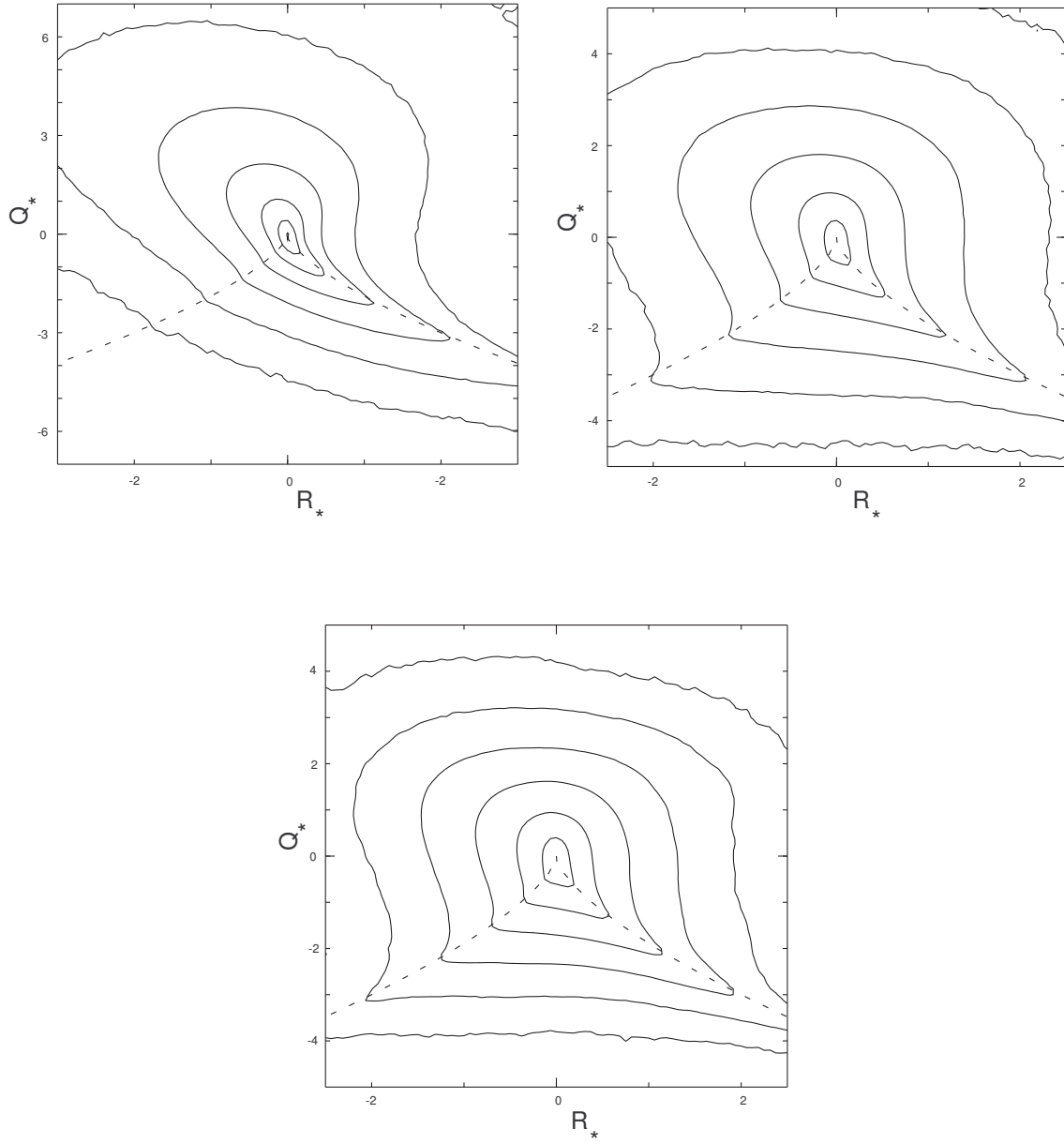


FIG. 3. The PDF of Q_* , R_* invariants normalized to the variance of strain, $Q_* \equiv Q / \langle s^2 \rangle$ and $R_* \equiv R / \langle s^2 \rangle^{3/2}$ ("star" denotes normalization), obtained from DNS at $R_\lambda = 85$ measured at different length scales: a) dissipation range $\rho = 2\eta$ b) low end of the inertial range $\rho = 8\eta$, and c) upper end of the inertial range $\rho = L/2$. The isoprobability contours are logarithmically spaced, and are separated by factors of 10. The dashed line corresponds to zero discriminant.

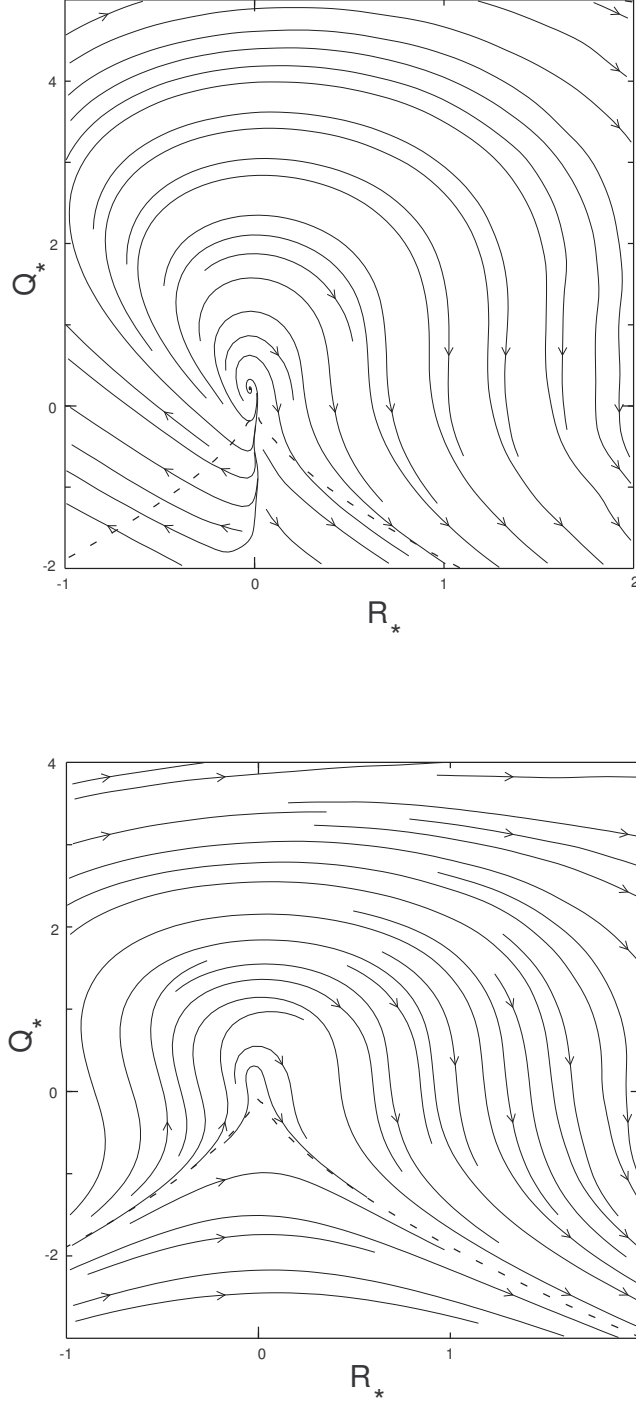


FIG. 4. Streamlines of the flow of M -invariants, constructed from the conditional $\langle \dot{Q}|Q, R \rangle$ and $\langle \dot{R}|Q, R \rangle$ measured from DNS at different length scales: a) dissipative range $\rho = 2\eta = L/32$, b) upper end of the inertial range $\rho = L/2$. The invariants R and Q are normalized as in Fig.3.

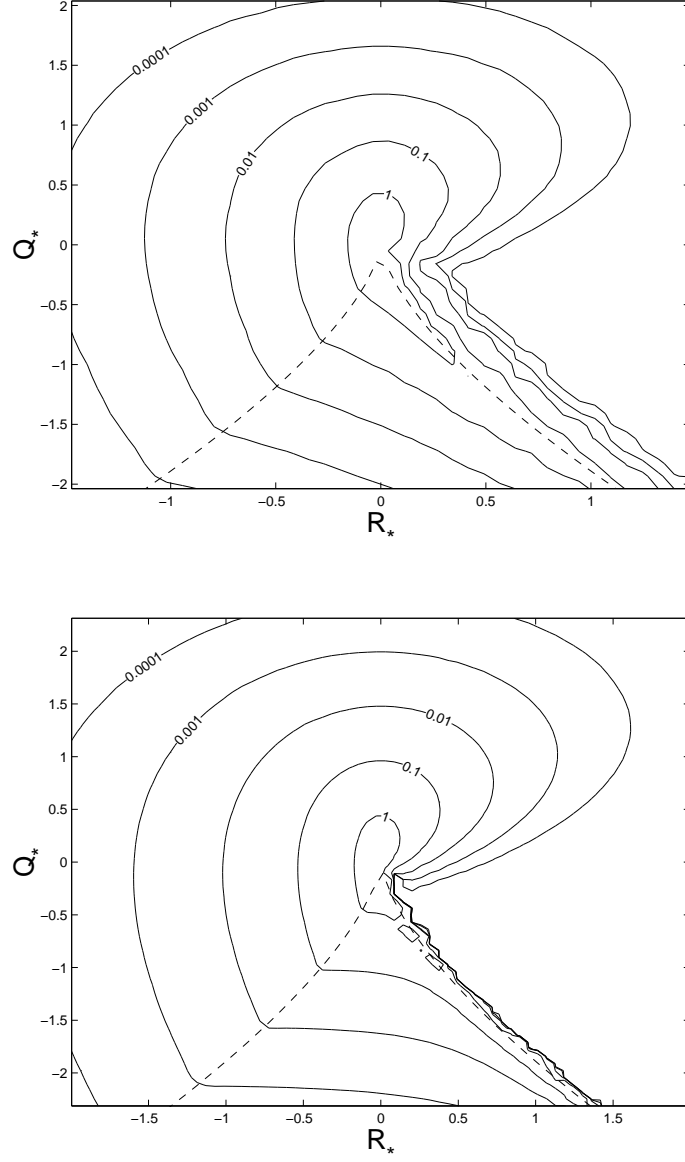


FIG. 5. PDF of Q_*, R_* invariants (normalized as in Fig.3) calculated for the tetrad model in the deterministic approximation
a) $\rho/L = .2$; b) $\rho/L = .5$.

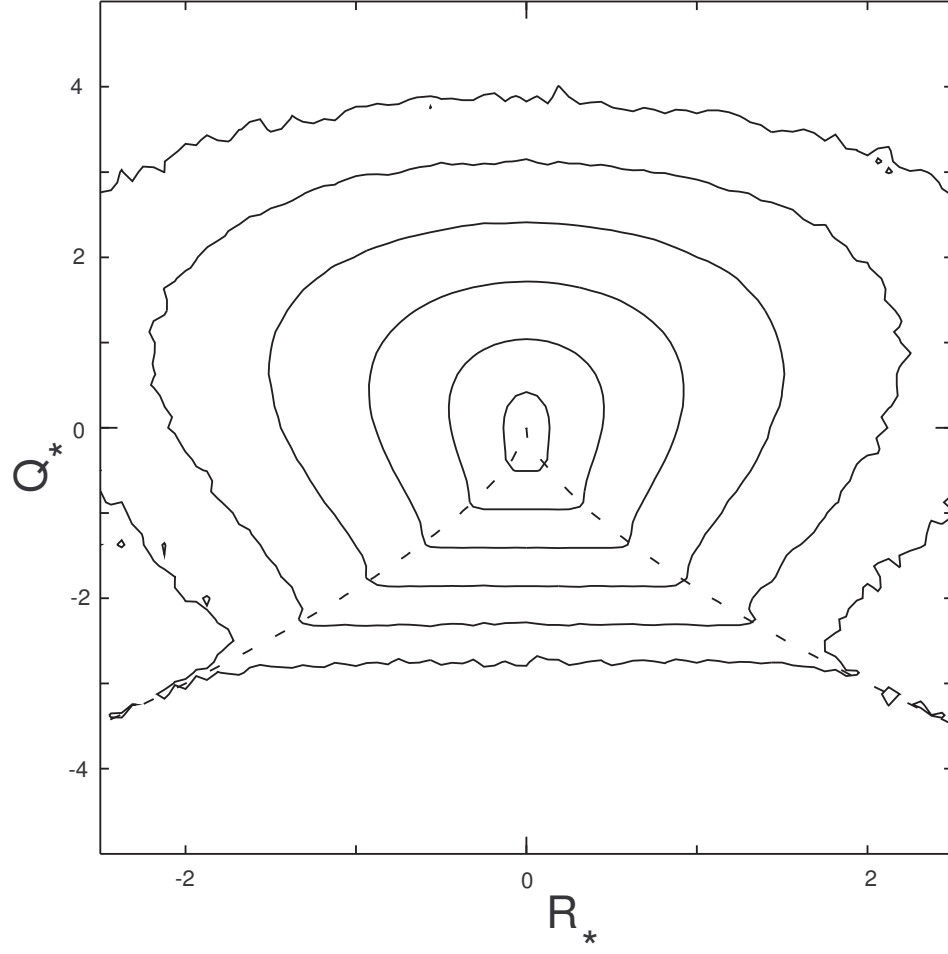


FIG. 6. The PDF of Q_* , R_* invariants (normalized as in Fig.3) obtained by replacing the real (DNS) velocity field by a random Gaussian field, with the same velocity spectrum.

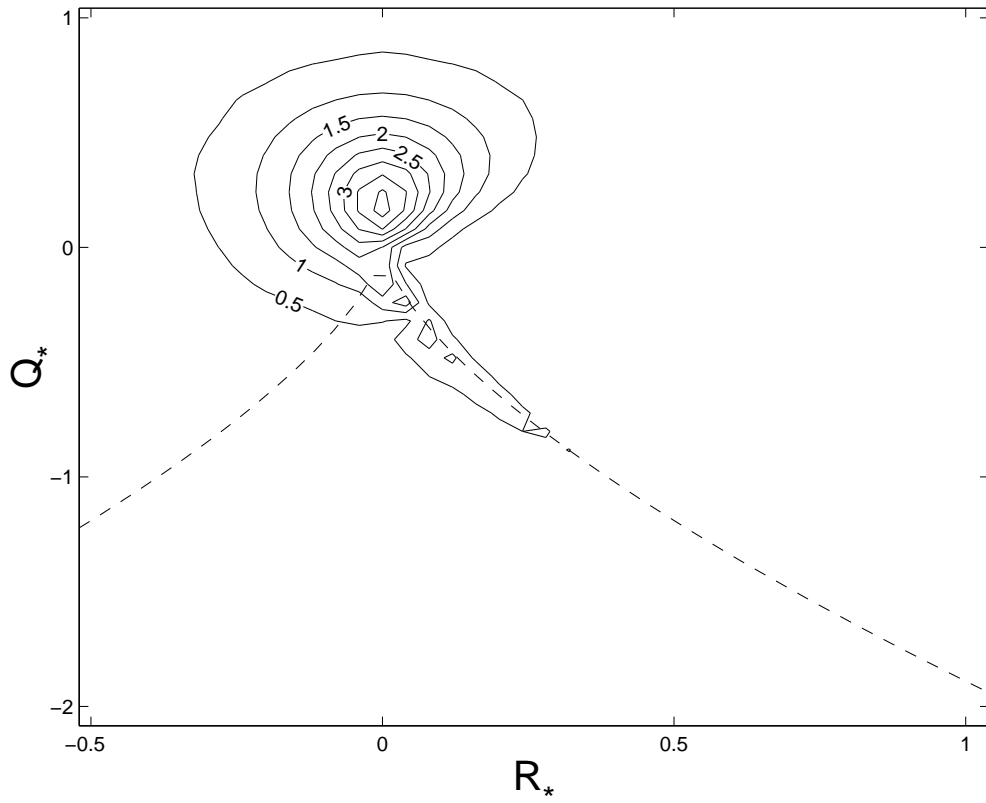


FIG. 7. Enstrophy density in R, Q plane for the tetrad model at $\rho/L = .5$

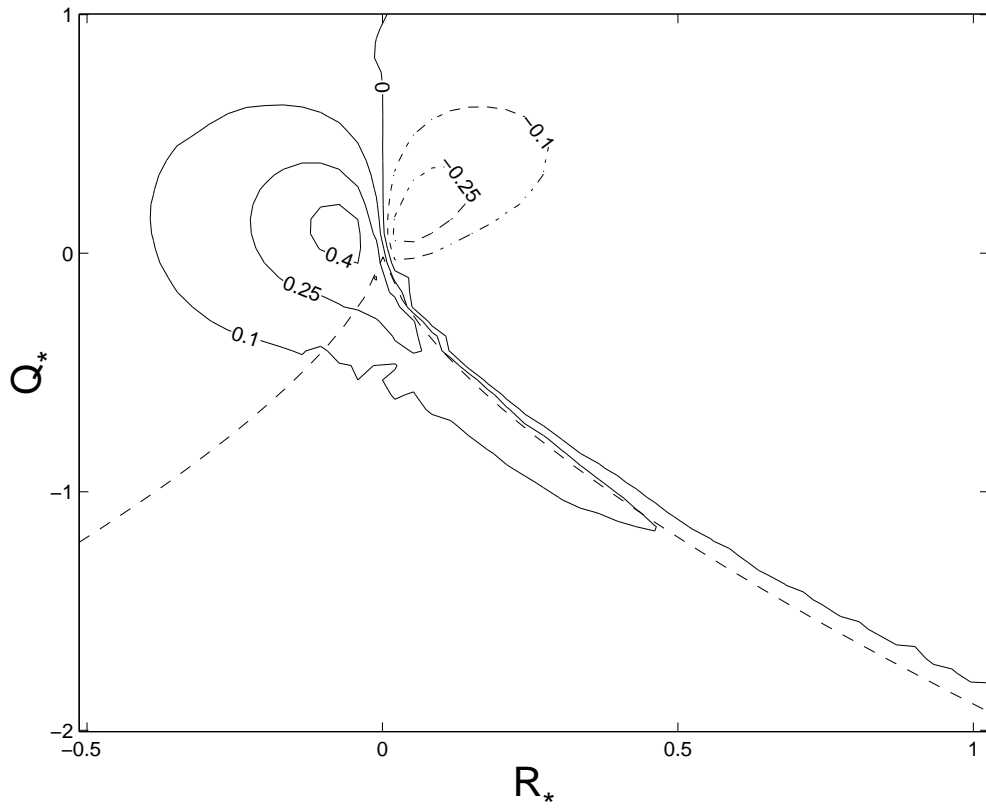


FIG. 8. Enstrophy production density in R, Q plane for the tetrad model at $\rho/L = .5$

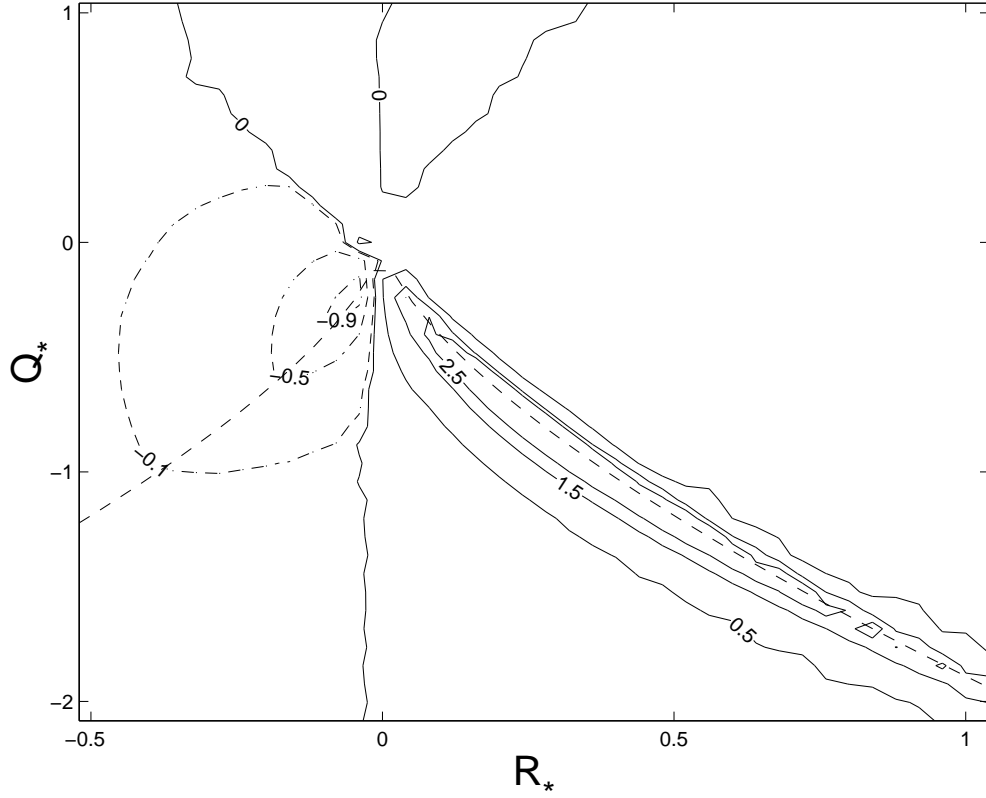


FIG. 9. Strain skewness density in R, Q plane for the tetrad model at $\rho/L = .5$

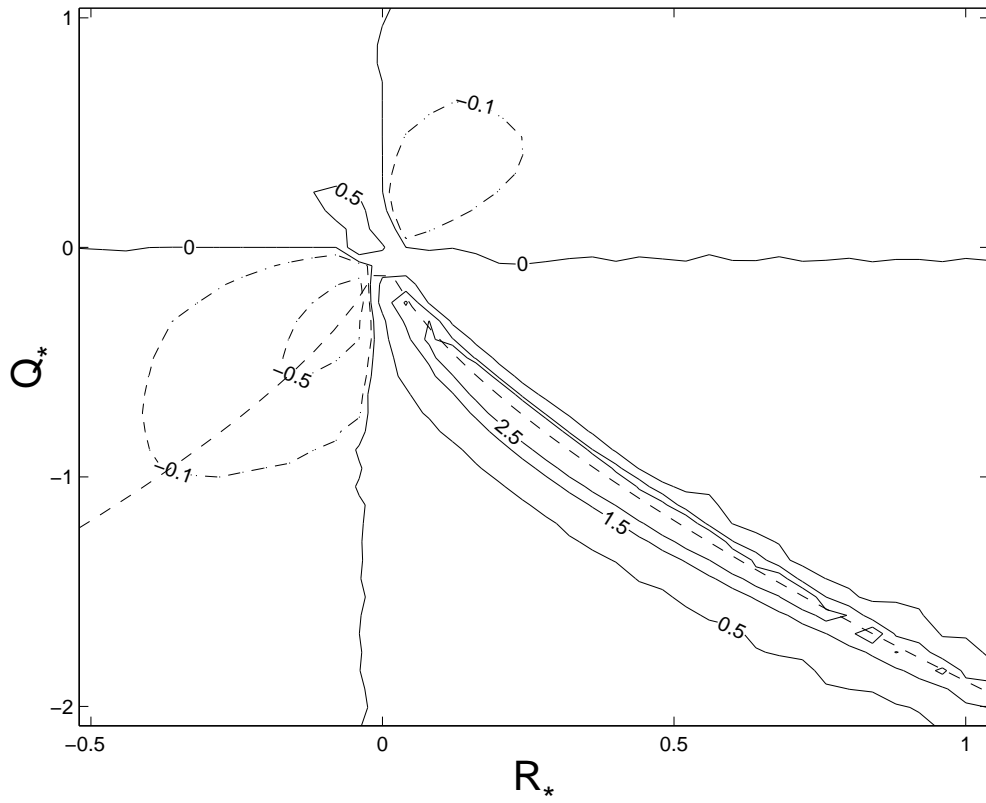


FIG. 10. Energy flux density in R, Q plane for the tetrad model at $\rho/L = .5$

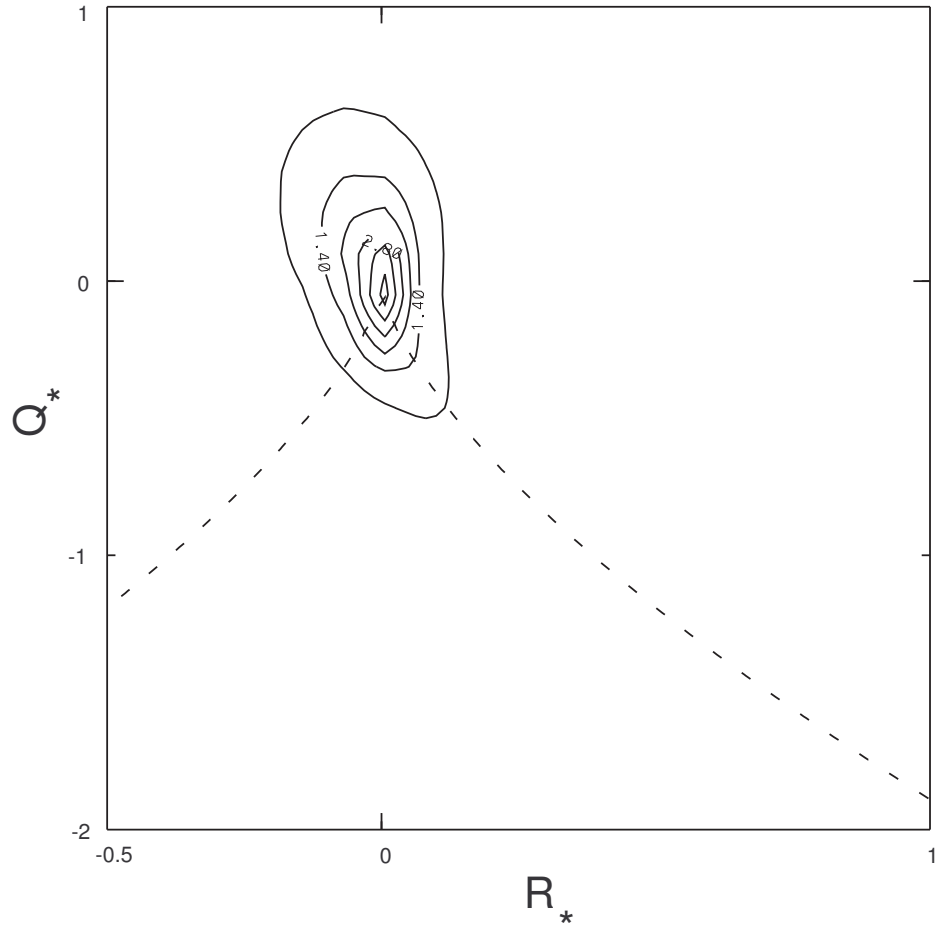


FIG. 11. Enstrophy density in R, Q plane from the DNS, $R_\lambda = 85$, at $\rho/L = 0.125$ (same value as in Fig.3c,4c). The enstrophy is normalized by $-2 < tr(\Omega^2) >$.

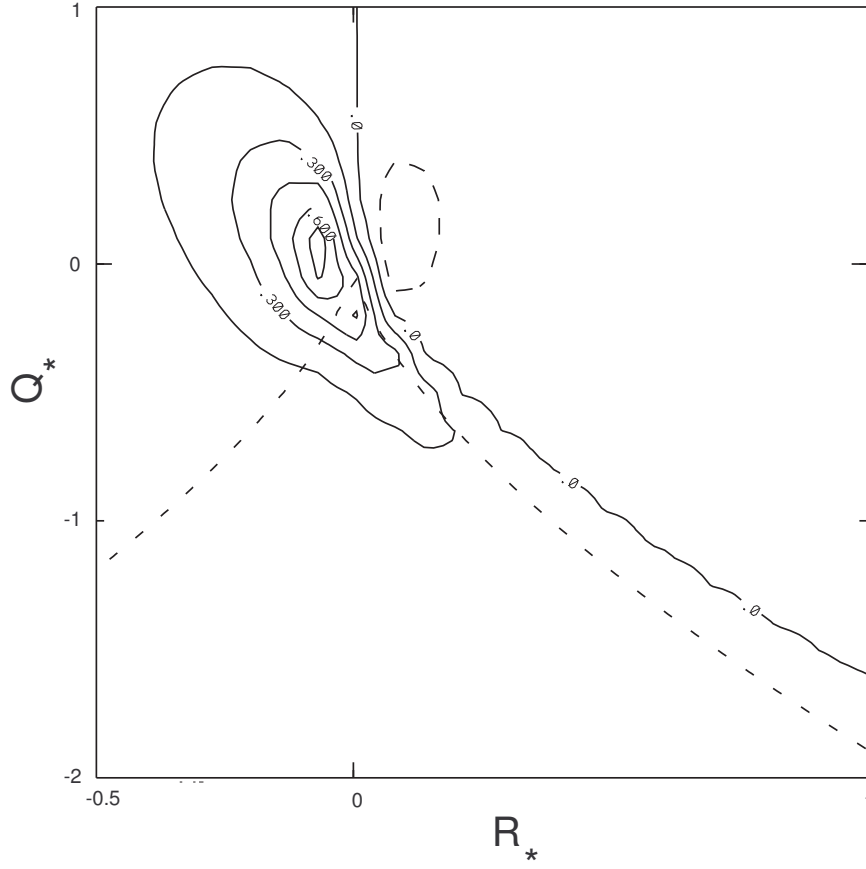


FIG. 12. Enstrophy production density in R, Q plane from the DNS, $R_\lambda = 85$, at $\rho/L = 0.125$. The enstrophy production is normalized by $|\langle tr(M^2 M^\dagger) \rangle|$. Solid lines correspond to positive values, dashed lines to negative values.

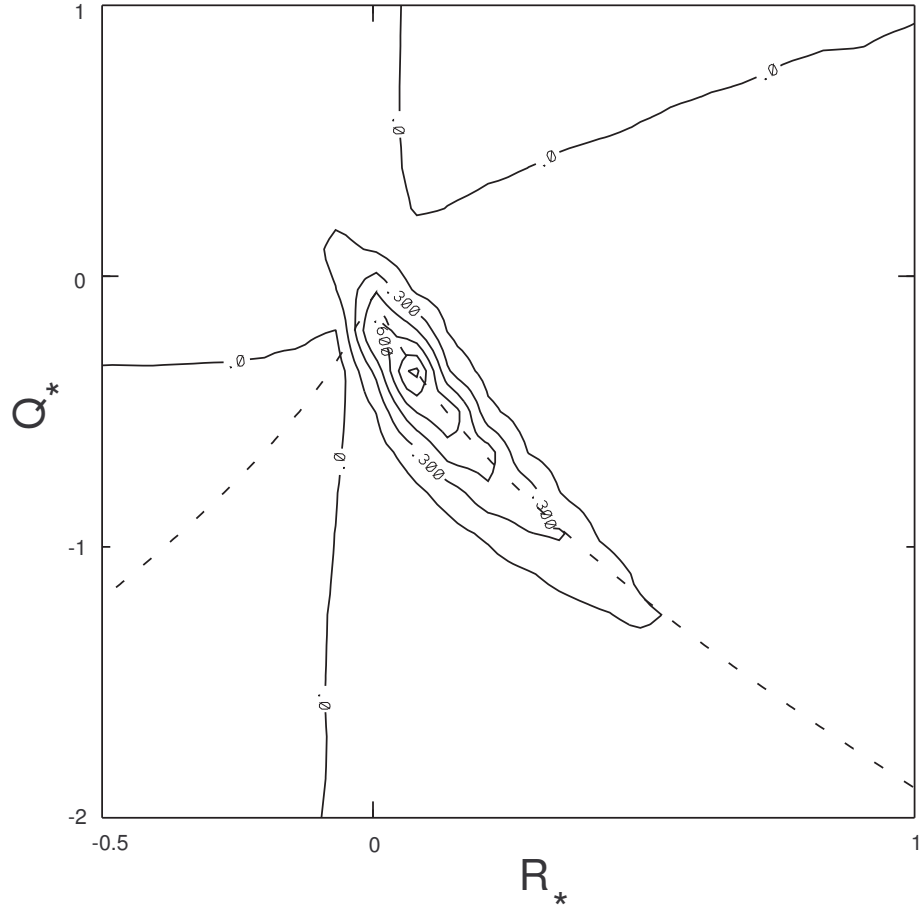


FIG. 13. Strain skewness density, $-tr(S^3)$ in R, Q plane from the DNS, $R_\lambda = 85$, at $\rho/L = 0.125$. The strain skewness density is normalized by $|\langle tr(M^2 M^\dagger) \rangle|$. The same convention as in Fig.12 is used.

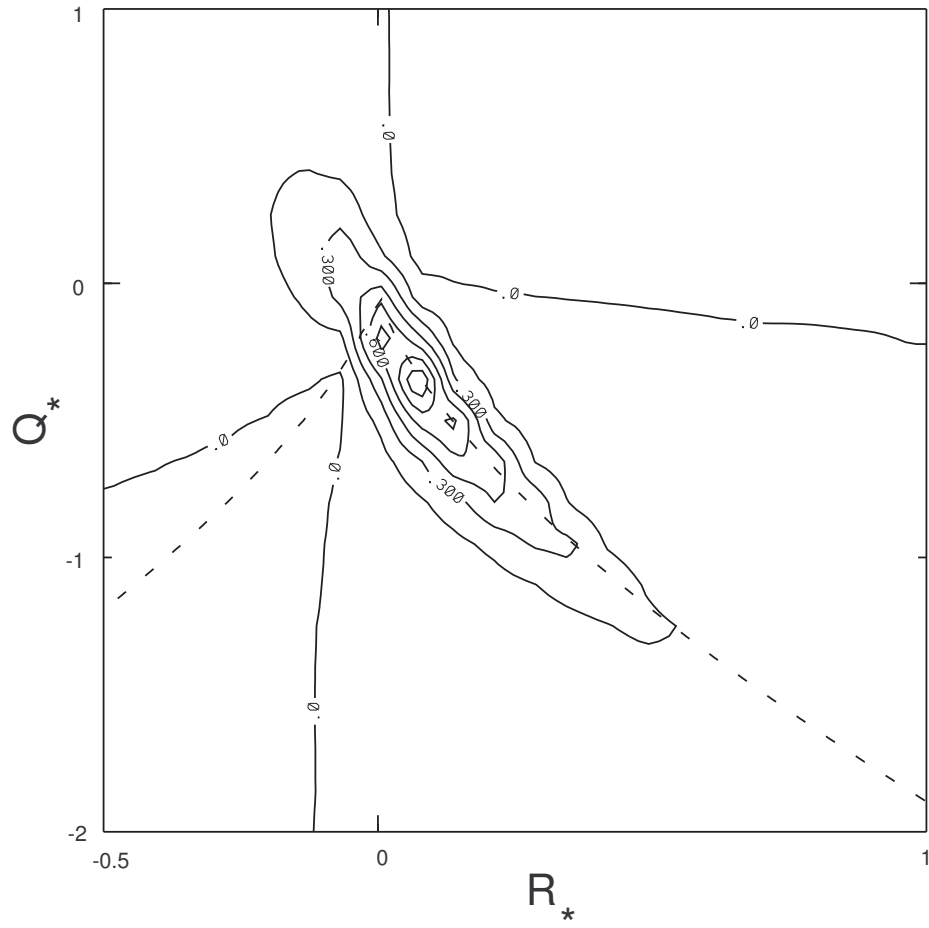


FIG. 14. Energy flux density, $tr(M^2 M^\dagger)$ in R, Q plane from the DNS, $R_\lambda = 85$, at $\rho/L = 0.125$. The energy flux density is normalized by $|\langle tr(M^2 M^\dagger) \rangle|$. The same convention as in Fig.12 is used.

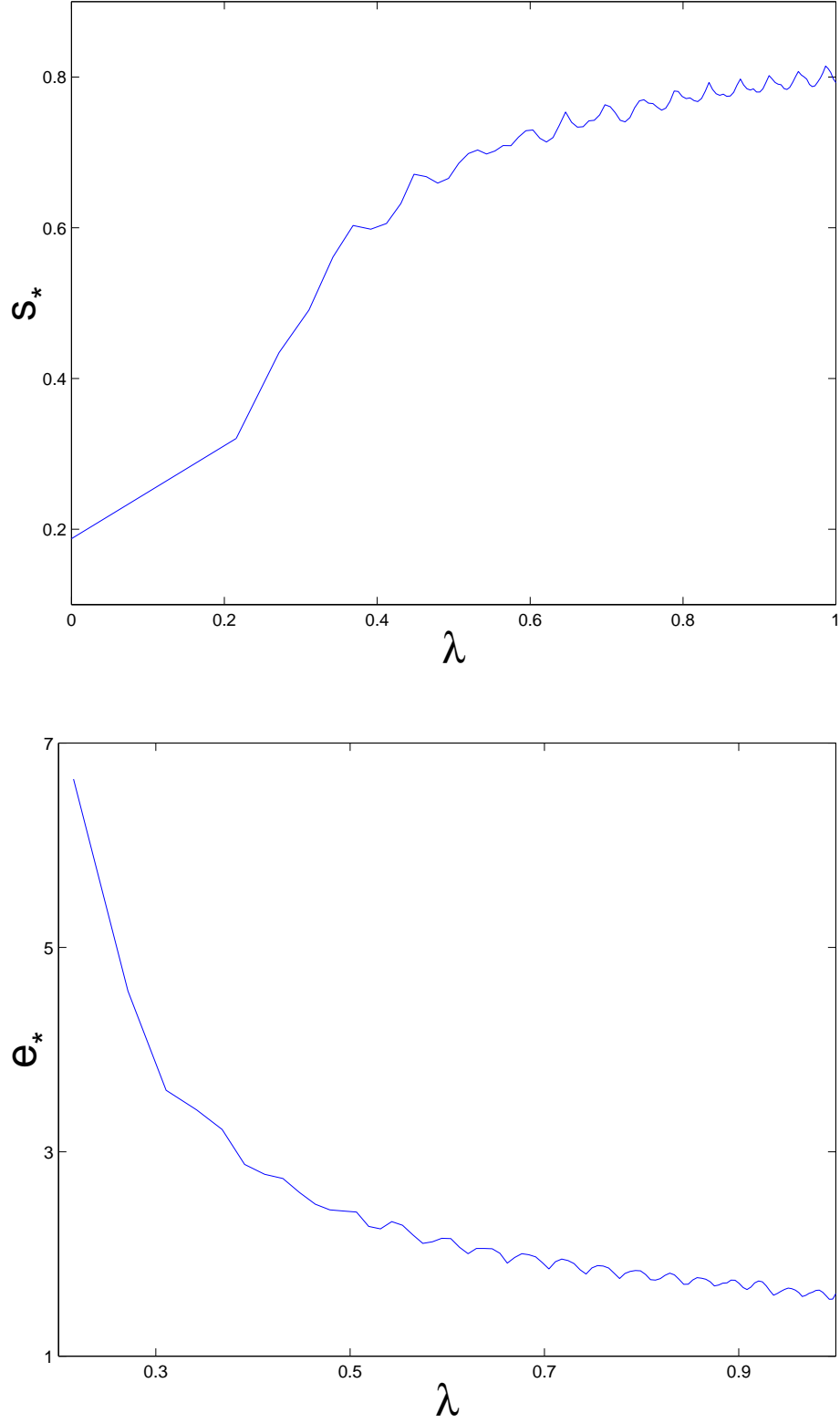


FIG. 15. a) Normalized intermediate eigenvalue of the strain , $s_* \equiv [6s_\beta]^{1/2}/|s|$, as a function of λ along the Vieillefosse tail as observed in the DNS, $R_\lambda = 85$, $\rho = 2\eta$; b) same for normalized enstrophy, $e_* \equiv \langle \omega^2 | \lambda \rangle / \lambda^2$, as a function of λ .

β	0.05	0.1	0.15	0.2	0.25	0.3
α	0.29	0.24	0.19	0.14	0.07	0.005
γ_+	0.05	0.11	0.18	0.25	0.33	0.43
η	1.11	1.14	1.21	1.28	1.35	1.44
ζ	1.95	1.86	1.71	1.66	1.63	1.55
δ	1.33	1.69	1.69	1.85	1.89	1.90
η'	0.27	0.22	0.34	0.34	0.42	0.52
n_c	62.98	28.87	18.82	12.88	9.92	7.52

Table 1 Table of exponents for the $D = 0$, $R > 0$ tail in the deterministic limit (Appendix A).